TECHNISCHE UNIVERSITÄT WIEN

Master Thesis

Development of an Energy Management Strategy for Fuel Cell Electric Vehicles considering Efficiency and Degradation of the Fuel Cell Stack

carried out for the purpose of obtaining the degree of Diplom-Ingenieur (DI),

submitted at TU Wien

Faculty of Mechanical and Industrial Engineering

by

Clemens Carl Maria KARNER, BSc

Mat.No.: 01126544

under the supervision of

Associate Prof. DI Dr.techn. Peter Hofmann

and

DI Dr.techn. Christoph Steindl, BSc

Institute of Powertrains and Automotive Technology, E315

Vienna, 4. June 2024 B24007

TECHNISCHE UNIVERSITÄT WIEN
Vienna University of Technology

IFA
Institut für Fahrzeugantriebe & Automobiltechnik

Aufgabenstellung für die Diplomarbeit

Herrn Clemens Carl Maria Karner, Matrikelnummer: 011 26 544 wird folgende Aufgabe gestellt:

„Entwicklung einer Betriebsstrategie für Brennstoffzellenfahrzeuge unter Berücksichtigung von Effizienz und Degradation des Brennstoffzellen-Stacks“

Es ist ein Simulationsmodell eines Brennstoffzellenfahrzeuges im Hinblick auf die spezielle Aufgabenstellung zu erstellen und Simulationsrechnungen zur Betriebsstrategieentwicklung hinsichtlich Absenkung von Kraftstoffverbrauch und Minimierung der Alterung des Brennstoffzellen-Stacks durchzuführen.
Fokus der Untersuchung soll die Analyse des Trade-off Verhaltens von Effizienz und Degradation des Brennstoffzellen-Stacks (BZ-Stacks) sein. Für den Vergleich mit einem bereits bestehenden Brennstoffzellenfahrzeug der oberen Mittelklasse sollen möglichst reale Komponenten und der Fahrzyklus WLTC verwendet werden.

Schwerpunkte:

- Erstellung eines Längsdynamikmodells des Brennstoffzellenfahrzeuges in AVL Cruise M
- Literaturrecherche bezüglich der Alterung von Brennstoffzellen
- Modellierung der Alterung eines BZ-Stacks
- Entwicklung einer Betriebsstrategie
- Gewichtung der Betriebsstrategie jeweils zur Minimierung des Verbrauchs sowie Reduktion der Alterung des BZ-Stacks
- Validierung des Modells anhand von Daten eines vergleichbaren Brennstoffzellenfahrzeuges im WLTC

Ein gebundenes Exemplar und eine Version der Diplomarbeit auf Datenträger sind am Institut für Fahrzeugantriebe und Automobiltechnik der Technischen Universität Wien abzugeben.

Juni 2024 B24007

Dauer: März 2021 - Juni 2024

Kennzahl: E 066445

Die Ergebnisse der Arbeit sind vertraulich zu behandeln und dürfen nur mit schriftlicher Genehmigung des Institutsvorstandes weitergegeben bzw. veröffentlicht werden.

Die Benutzung der Versuchseinrichtungen des Institutes hat in den Dienststunden und unter Anleitung des Betreuers zu erfolgen. Dabei dürfen alle Arbeiten nur unter besonderer Beachtung der geltenden Sicherheitsvorschriften durchgeführt werden.

Einverstanden:

Clemens Carl Maria Karner, BSc

Betreuender Assistent:

DI Dr. Christoph Steindl

Betreuer und Institutsvorstand:

Assoc. Prof. DI Dr. Peter Hofmann

Juni 2024

B24007

I confirm, that the printing of this thesis requires the approval of the examination board.

Affidavit

I declare in lieu of oath, that I wrote this thesis and carried out the associated research myself, using only the literature cited in this volume. If text passages from sources are used literally, they are marked as such.

I confirm that this work is original and has not been submitted for examination elsewhere, nor is it currently under consideration for a thesis elsewhere.

I acknowledge that the submitted work will be checked electronically-technically using suitable and state-of-the-art means (plagiarism detection software). On the one hand, this ensures that the submitted work was prepared according to the high-quality standards within the applicable rules to ensure good scientific practice "Code of Conduct" at the TU Wien. On the other hand, a comparison with other student theses avoids violations of my personal copyright.

Place and Date *Signature*

Acknowledgements

I would like to particularly thank Bernhard Geringer and Peter Hofmann for the opportunity to investigate the topic of this thesis, which is of special interest to me personally.

Christoph Steindl and Maximilian Haslinger have been a great support to me in every detail of my subject matter, and they also shared their positive and inspiring opinions with me - thank you.

Thanks to everybody from the TU Wien for their support of distance learning during Covid-19, which allowed me to continue with my studies throughout the crisis.

Last but not least, I am grateful for my wife Laura. Without her support, I would not have managed to finish my diploma thesis.

Abstract

A reaction to the society's call for mitigation of the climate change could be the use of renewably produced hydrogen in Fuel cell hybrid electric vehicles (FCHEVs) as emission free means of transportation. They are being heavily investigated, from system architectures in general, to improvements of their components. The ambition is to reach broad customer acceptance due to lowered costs, more convenient and robust operation, and longer lifetime.

In this work a longitudinal dynamics simulation model of a fuel cell (FC) hybrid electric vehicle is set up in the software environment AVL Cruise M. It is parametrised and validated with measurement results of a first generation Toyota Mirai on the Institut für Fahrzeugantriebe und Automobiltechnik (IFA)/TU Wien chassis dynamometer and a standalone fuel cell system on the IFA/TU Wien fuel cell system test stand. The vehicle model incorporates a fuel cell degradation model, which is developed from the results of a literature survey. An energy management strategy (EMS) is developed, which comprises parameter-controlled functions for load shifting and phlegmatisation of the proton-exchange-membrane fuel cell stack's power demand.

The vehicle model is studied in the WLTC-3b driving cycle to qualitatively identify potential gains in fuel cell lifetime, while preserving high fuel efficiency. The EMS's parameters are numerically optimised in several runs, to obtain a minimum fuel consumption benchmark case, a minimum fuel cell degradation case, and to elaborate the trade-off behaviour between these two benchmarks.

The results point towards attractive gains in potential fuel cell lifetime at the cost of only a minor increase in fuel consumption. Furthermore, this work presents a parametrisable fuel cell degradation evaluation tool, which can easily be updated with future research findings to investigate other fuel cell systems. Besides that, the validated vehicle model can be used for future assessments of other EMS's basic structures.

Kurzfassung

Der gesellschaftliche Ruf nach einer Entschleunigung des Klimawandels wird immer lauter. Mit nachhaltig hergestelltem Wasserstoff betriebene Brennstoffzellenfahrzeuge bieten eine Möglichkeit, Treibhausgas-Emissionen im Transportsektor zu reduzieren, da sie im Betrieb keine Emissionen freisetzen. Sie stehen im Fokus aktueller Forschungsarbeiten, um ihre Kundenakzeptanz durch Kostensenkung, Systemvereinfachung, sowie längere Lebensdauern zu erhöhen.

Diese Arbeit präsentiert ein längsdynamik Simulaionsmodell eines Brennstoffzellen Hybridfahrzeugs, entwickelt in der Softwareumgebung AVL Cruise M. Zur Parametrierung und Validierung der Submodelle dienen Messdaten des Toyota Mirai der ersten Generation am IFA/TU Wien Rollenprüfstand und des IFA/TU Wien Brennstoffzellensystemprüfstands. Ein Alterungsmodell für Brennstoffzellen wird basierend auf den Ergebnissen einer Literaturrecherche erstellt und in das Fahrzeugmodell eingebunden. Die für das Modell entwickelte Betriebsstrategie beinhaltet parametergesteuerte Funktionen zur Lastpunktverschiebung und zur Phlegmatisierung der Leistungsanforderung an den Polymerelektrolyt-Membran Brennstoffzellenstack.

Das Fahrzeugmodell wird mittels des WLTC-3b Fahrzyklus untersucht, um die unter Beibehaltung möglichst hoher Kraftstoffeffizienz erzielbare Milderung der Brennstoffzellenalterung qualitativ zu bewerten. Die numerische Parameteroptimierung der Betriebsstrategie liefert Referenzwerte für minimalen Kraftstoffverbrauch und minimale Brennstoffzellenalterung des gegebenen Systems. Darüber hinaus wird das Trade-off Verhalten zwischen diesen beiden Referenzwerten untersucht.

Die Ergebnisse deuten auf eine große mögliche Reduktion der Alterung hin, während dafür nur ein geringfügig höherer Kraftstoffverbrauch in Kauf genommen werden muss. Außerdem bietet das vorgestellte Alterungsmodell für Brennstoffzellen die Möglichkeit, die Ergebnisse künftiger Forschungsarbeiten einzupflegen und damit andere Brennstoffzellensysteme zu untersuchen. Das validierte Fahrzeugmodell kann überdies zur weiteren Entwicklung und Bewertung von alternativen Betriebsstrategieansätzen verwendet werden.

Contents

Abbreviations

ADAC	Allgemeiner Deutscher Automobil-Club
AFC	Alkaline fuel cell
ASM	Asynchronous machine
BAB	Bundesautobahn driving cycle
BoL	Beginning of life
BoP	Balance of plant
CADC	Common Artemis Driving Cycles
CHSS	Compressed hydrogen storage system
CO_2	Carbon dioxide
DC	Direct current
DE	Differential evolution
DLFC	Direct liquid fuel cell
DMFC	Direct methanol fuel cell
ECMS	Equivalence consumption minimisation strategy
EESM	Electrically excited synchronous machine
EM	Electrical machine
EMS	Energy management strategy
EoL	End of life
FC	Fuel cell
FCHEV	Fuel cell hybrid electric vehicle
FCS	Fuel cell system
H_2	Hydrogen
HV	High-voltage
MCFC	Molten carbonate fuel cell
MEA	Membrane electrode assembly
NEDC	New European Driving Cycle
NiMH	Nickel metal hydrid
PAFC	Phosphoric acid fuel cell
PEMFC	Proton-exchange-membrane fuel cell
PMSM	Permanent magnetic synchronous machine
SoC	State of charge
SOFC	Solid oxide fuel cell
WLTC-3b	Worldwide harmonised Light vehicles Test Cycle for class 3b vehicles

1 Introduction

Climate change advances globally. The emissions of greenhouse gases caused by human activity are considered a major cause for the increasing ambient temperatures worldwide. Carbon Dioxide (CO_2) accounts for a large proportion of the observed impact on the environment. With advancing globalisation, the volume of transport is also increasing. Consequently, a further increase in CO_2 emissions is expected, as most vehicles currently run on fossil fuels.

Today there is a range of possibilities available to mitigate CO_2 emissions from the transport sector. One of the most promising technologies for vehicle propulsion without locally generated emissions, is the use of renewably produced hydrogen as energy carrier in fuel cell hybrid electric vehicles (FCHEVs). Water vapour and ambient air are the only substantial exhaust gas components of a proton-exchange-membrane fuel cell (PEMFC) in an FCHEV. The chemically stored energy of hydrogen is directly converted into electricity and heat within the PEM fuel cell (FC) stack. In turn, the electrical energy is used in the vehicle's electric machine (EM) to provide traction power or is buffered into the onboard high-voltage (HV) battery.

PEMFCs are subject of ever-increasing research and development. Researchers are in the process of getting insight into the behaviour of the most commonly used fuel cell type in vehicles, the PEMFC. Main research topics are the further improvement in the balance of plant (BoP) components, as well as further investigation of stack design, single cell components, materials, and their manufacturing processes [1]. This work builds on existing research data, and presents an abstract fuel cell degradation model.

Fuel cells degrade over their lifetime. They lose efficiency and performance or even fail catastrophically, while different mechanisms cause the degradation of the stack at specific operating points and during certain operating conditions [1–3]. The end of life (EoL) of a fuel cell can be defined by a specific loss of performance, compared to the beginning of life (BoL). The long-term development objective for light duty vehicles is set to 6000 operating hours, according to the HORIZON 2020 programme of the European Union [4].

In the presented work, longitudinal dynamics simulation calculations of a PEMFC in an FCHEV are conducted. The main focus is the evaluation of the potential to enhance the expectable FC stack lifetime, while maintaining the maximum possible fuel efficiency, within the given framework. The model of an upper middle-class FCHEV is created and validated with data from a measurement of a first generation Toyota Mirai in the ADAC Eco Test cycle on the IFA/TU Wien chassis dynamometer. This electromechanical model is paired up with a scaled-up version of a standalone fuel cell system, which has been investigated by other researchers on the IFA/TU Wien fuel cell system test stand. Thereby

obtained measurement data provides the basis for the parametrisation of an equivalent circuit fuel cell stack model, and for the implementation of its ancillaries via a lookup table. The insights of a literature survey are used to retrieve a data-driven fuel cell degradation model, which runs in parallel with the vehicle model. It yields a representative single cell potential loss at a reference load level. For the investigations in this work, the Worldwide Harmonized Light Vehicles Test Cycle for class 3b vehicles (WLTC-3b) is chosen as the driving profile.

The vehicle model's energy management strategy (EMS) controls the full functional range of the drivetrain. It also decides about the power split between the fuel cell stack, and the HV battery, to meet the traction power requested by the driver. Therefore it plays a crucial role for the fuel consumption and FC stack degradation, as it determines the operation of the fuel cell stack [5]. The EMS is specifically designed and developed for the flexibility to adopt its behaviour according to the desired objective compromise.

The objectives of minimum fuel consumption and minimum fuel cell degradation are contrary: Possible gains in stack lifetime have to be "bought" with an increased fuel consumption. An optimisation algorithm is used to refine parameters of the EMS, with the aim of creating benchmark results for the minimum possible fuel consumption and minimum possible fuel cell degradation - considering the implemented strategy. The resulting trade-off behaviour between both objectives is elaborated by adjusting the weighting of each individual objective in a specifically developed overall objective function.

2 Literature Review and State of the Art

This chapter sheds light on the state of the art of FCHEVs and their main components. Today's knowledge about fuel cell degradation is summarised, as well as energy management strategies are explained in general. This chapter therefore provides the base for the assumptions and simplifications made in the modelling of the vehicle's propulsion system components and the fuel cell degradation model.

2.1 Fuel Cell Hybrid Electric Vehicles

Generally, hybrid vehicles are substantially different from conventional road vehicles with a single power source, as hybrids feature at least two energy sources and energy converters on board. A special class of hybrid vehicles is that of fuel cell hybrid electric vehicles. Those operate without locally producing pollutant or greenhouse gas emissions. Besides a fuel cell system (FCS), FCHEVs are equipped with a second energy source. Such energy sources may consist of either batteries, ultra-capacitors, or a combination thereof [6, 7]. To point out trendsetting technologies, a selection of commercially available passenger FCHEVs and their respective technical key data is provided in Table 2.1.

The conclusion of the data, given in Table 2.1, is that PEMFCs and 70 MPa compressed hydrogen storage systems (CHSSs) are state of the art. Batteries as secondary energy storage are the industrial standard, although their sizing and formulation differs between the competing models. The FCS output power is generally designed smaller than that of the electrical machine. The FCS vs. motor power share ranges from 48.4 % for the Mercedes Benz GLC F-Cell to over 100 % for the first generation Toyota Mirai respectively. Furthermore, a fuel cell stack, consisting of around 330 to 440 cells, seems to be the limit of what is feasible to fit in the chassis concepts. Besides that, it looks like a driving range of approximately 500 to 600 km is a common design ambition, bearing in mind that the data is given for different or unknown driving cycles. From Table 2.1, both Hyundai exemplars do not use a DC/DC-boost converter for the fuel cell stack, but all other models do. Such boost converters are used to lower the amperage in the HV system, therefore reducing size and material consumption of the electrical machine and the wiring. On the other hand, these converters need space by themselves, and they are considered a significant part of the overall vehicle cost and development efforts. The electrical machines, used among the different models, are the electrically excited synchronous machine (EESM), the permanent magnetic synchronous machine (PMSM), and the asynchronous machine (ASM).

Table 2.1: Latest FCHEVs and their key data.

Car / Type / Year	Electrical machine	Fuel cell stack	Secondary energy storage	Hydrogen storage system	Cruising range
Honda Clarity Fuel Cell / Sedan / 2017 [8, 9]	130 kW; EESM	358 cells; 103 kW; PEM	1.7 kWh [1]; Li-ion battery	5.46 kg; 70 MPa	650 km; NEDC
Hyundai ix35 Fuel Cell / SUV / 2015 [10, 11]	100 kW; ASM	433 cells; 100 kW; PEM	0.95 kWh; Li-ion-polymer battery	5.6 kg; 70 MPa	427 km; unknown cycle
Hyundai Nexo / SUV / 2018 [12, 13]	120 kW; PMSM	440 cells; 95 kW; PEM	1.56 kWh; Li-polymer battery	6.3 kg; 70 MPa	666 km; converted to NEDC
Mercedes Benz GLC F-Cell / SUV / 2018 [14, 15]	147 kW; ASM	412 cells; 75 kW; PEM	13.8 kWh; Li-ion battery	4.4 kg; 70 MPa	486 km; NEDC
Toyota Mirai / Sedan / 2014 [14, 16]	113 kW; PMSM	370 cells; 114 kW; PEM	1.6 kWh; NiMH battery	4.9 kg; 70 MPa	482 km; unknown cycle
Toyota Mirai II / Sedan / 2020 [17, 18]	134 kW; PMSM	330 cells; 128 kW; PEM	1.24 kWh; Li-ion battery	5.6 kg; 70 MPa	650 km; WLTC

Detailed measurement data of the first generation Toyota Mirai [22] is available for the author, hence that vehicle is chosen to be the reference throughout the work. Figure 2.1 shows the layout of its powertrain architecture and power type of each component.

The main components of the Mirai's fuel cell system are the fuel cell stack and its electrically driven ancillaries. These are a coolant pump, a hydrogen recirculation pump and an air compressor. Besides the battery cells themselves, the on board HV battery system contains protection circuitry, and it is air cooled. A PMSM is the vehicle's traction motor. Further components worth noting are the air conditioning compressor, an electrical heater, and a 12 V cabin consumer system (labelled "12 V loads" and "12 V battery" in Figure 2.1). As seen in Figure 2.1, most of the components do not work at the same

[1] Capacity according to no longer available original source [19] in [20]. Plausibilty check: The battery pack's nominal voltage of 364 V [9] could be yielded by 96 single cells at 3.6 V [21] nominal voltage. A 96s1p battery pack, with 5 Ah [21] single cell capacity, therefore has a total capacity of 1.7 kWh.

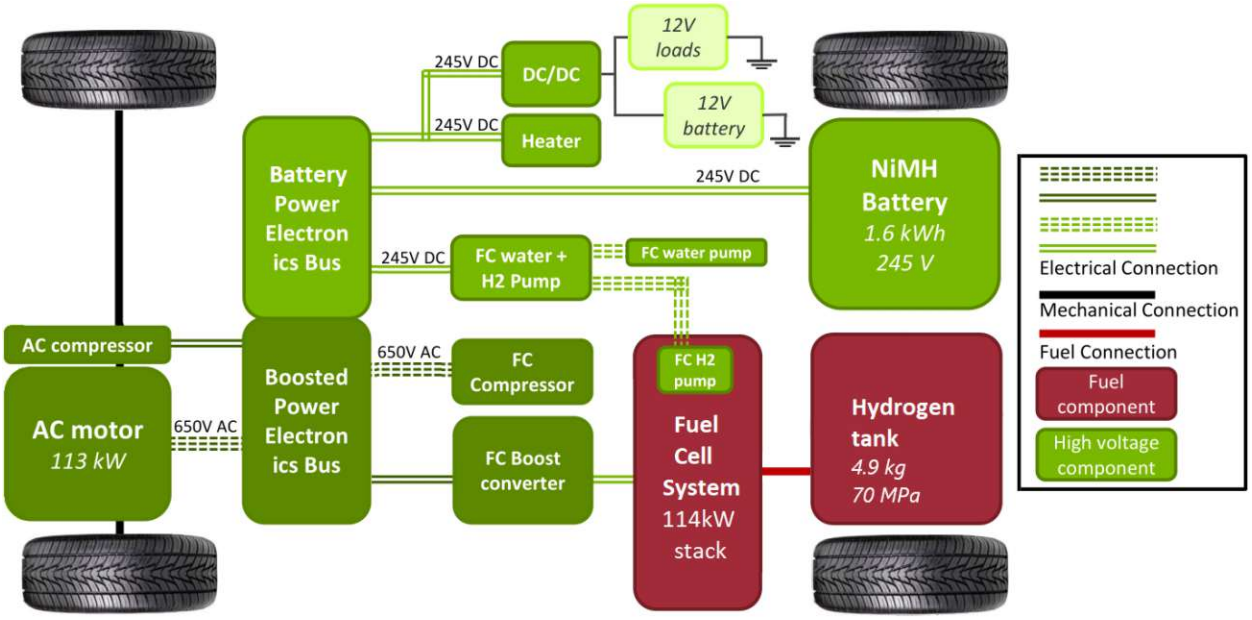

Figure 2.1: Scheme of a FCHEV's powertrain: The 2017 Toyota Mirai [16]. (modified representation)

voltage level nor current type. Power conditioning therefore takes on an important role, to provide direct current as well as three-phase alternating current at the correct voltage level to the different consumers [6, 16]. That in turn implies losses at every necessary conversion throughout the vehicle's electrical power distribution net.

Within given limits to power demand, both the fuel cell system, and the HV-battery can power the Mirai on their own. The Mirai´s powertrain architecture can therefore be classified as serial hybrid, with the FC system in combination with the hydrogen storage system being the primary energy source [6]. The decision about the load distribution between the HV-battery and the FCS is made by the energy management strategy. Section 2.2 takes a closer look at the most important physical components, whereas energy management strategies are considered in more detail in section 2.4.

2.2 Automotive Fuel Cell Systems

In this section, the requirements on fuel cell systems used in automotive applications are pointed out. The power demand requested on these systems usually is highly volatile and hardly predictable under real driving conditions. Together with widely spread operating conditions, that presents a major challenge for the overall FCS design process. The most important auxiliary components, which are needed to operate a fuel cell stack, are covered in this section as well.

Fuel Cell Types compared

All fuel cell types have one property in common. They are designed in a way, that some sort of fuel is spatially separated from an oxidant by an electrolyte. The type of electrolyte can be used to characterise the distinct types of fuel cells, as it determines core characteristics of the cell. Operating temperature, the demanded fuel and oxidant type and the electrochemical working principle are among the most determining properties [2, 14]. Table 2.2 provides an overview of the respective fundamental characteristics.

Table 2.2: Selection of principal fuel cell types [2].

Fuel cell (FC) type	Operating temperature (°C)	Mobile ion	Fuel
Alkaline (AFC)	50-200	OH^-	gaseous; H_2; pure
Proton-exchange-membrane (PEMFC)	30-100	H^+	gaseous; H_2, pure
Direct liquid (DLFC)	20-90	H^+	liquid; alcohols, other organic liquids
Phosphoric acid (PAFC)	220	H^+	gaseous; H_2, (low S, low CO, tolerant to CO_2)
Molten carbonate (MCFC)	650	CO_3^{2-}	gaseous or liquid; H_2, various hydrocarbon fuels (no S)
Solid oxide (SOFC)	500-1000	O_2^-	gaseous or liquid; impure H_2, variety of hydrocarbon fuels

From that list, the PEMFC is the only one used in large-scale production passenger cars for several reasons. A disadvantage of the SOFC, the MCFC and the PAFC is, that they have limited turn down ratios. That means, their minimum power output is relatively high, compared to their full load output. Thermal cycling causes severe performance loss, which is why these FCs are not able to fulfill the volatile power demand of a vehicle [14]. E.g. an experiment of 15 start-up and shut-down cycles shows performance deterioration for an SOFC, mostly caused by sealing problems and cracks due to different coefficients of thermal expansion of the stack's components [23]. One on-off-cycle takes approximately 1600 minutes for the SOFC in [23], which would be unacceptable for automotive applications. The PEMFC has a considerably lower operating temperature than the SOFC, MCFC and the PAFC. Starting up a PEMFC does therefore not take much time and it is less prone to failures due to start-stop temperature cycling [14].

The most mature developed DLFC is the direct methanol fuel cell (DMFC). As it can use a proton-exchange membrane as electrolyte, this fuel cell type is closely related to the PEMFC. But due to relatively low reaction rates for the direct oxidation of the liquid fuel, the specific power output is considerably lower than that of a gas fed fuel cell.

Even the benefits of system simplicity and the high gravimetric energy content of a liquid fuel can not outweigh that disadvantage for automotive applications [2, 14]. A number of variations of the AFC exist, which are at different stages of development. Besides the anion-exchange membrane fuel cell, all other AFC types lack of tolerance against CO_2 contaminations in the fuel or the oxidant supply. Carbonates are irreversibly formed in the electrolyte due to the presence of CO_2, which severely reduce cell performance. Working media purification against CO_2 therefore takes on an important role, which would increase system complexity in automotive applications. Carbonate precipitates cannot be formed in the membrane of a solid anion-exchange membrane fuel cell, but its ion conductivity is too low to consider it for other applications than e.g. water desalination [2].

2.2.1 Proton-Exchange-Membrane Fuel Cells and their Working Principle

Based on Figure 2.2, which shows a schematic cross section of a single cell within a cell stack, the basic components of a PEMFC stack are explained.

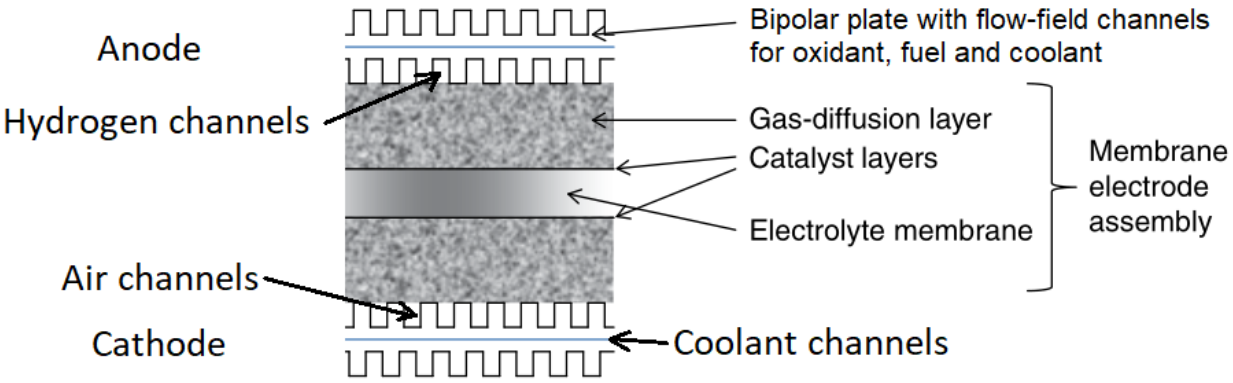

Figure 2.2: Schematic cross section of a single PEMFC within a cell stack [2]. (modified representation)

The basic mechanical components of a PEMFC are symmetrically arranged around the electrolyte membrane layer in the middle, as seen in Figure 2.2. The membrane is coated with catalyst layers, which are covered with highly porous gas diffusion layers. These five layers represent the membrane electrode assembly (MEA), which is contacted with grooved plates on each side. As one fuel cell only produces a voltage of roughly 0.5 - 0.9 V [22] during operation, they are electrically connected in series to provide power at a higher voltage level. The state of the art is to directly stack the MEAs, separated by so called bipolar plates. These plates electrically and mechanically connect the anode of one cell with the cathode of the cell next to it, and they introduce physical structure into the stack [2, 24].

A PEMFC is operated by feeding gaseous hydrogen to the anode side (negative pole) of the cell, and conditioned ambient air to the cathode side (positive pole) of the MEA. The

exothermic electrochemical global reaction, stated in Equation 2.1, consumes hydrogen from the anode and oxygen from the cathode to produce water on the cathode side of the cell. The simplified process for that reaction is, that hydrogen releases its electron at the anode and then moves through the electrolyte membrane as H^+-ion (proton). Arriving at the cathode side, these protons react with the surrounding oxygen molecules and absorb electrons again. The electrons have to travel through the external electric circuit, which connects the anode and cathode. This way, electrical power is supplied to the connected electrical loads [2].

The aim of providing hydrogen and oxygen to the catalyst layers in an efficient and uniform way is that the energy conversion can take place efficiently and evenly across the surface. The reactants and the coolant are provided to the MEAs through complex channel systems integrated in the bipolar plates, but also product water management takes on a major role for the flow field development [2, 25].

$$2\,\mathrm{H_2} + \mathrm{O_2} \iff {}_2\mathrm{H_2O} \tag{2.1}$$

The electrochemical Equation 2.1 describes the global reaction in a fuel cell and yields a theoretical cell potential E of approximately 1.2 V, for a cell that is operated below 100 °C [2]. Under realistic conditions, only a portion of that voltage level is achieved. Gathering a polarisation curve is a way to present a fuel cell's performance characteristics vividly. Furthermore, if cell-surface-normalised data is plotted, a comparison can be made between cells of different size.

The Electrochemistry of a Fuel Cell

A generic polarisation curve with a characteristic course is shown in Figure 2.3, where also the dominant loss mechanisms in their respective load regions are indicated [24].

In the low load region, activation losses are dominating the performance characteristic of the cell. The major cause therefore is the activation energy, which is needed to initiate a chemical reaction. The available terminal voltage is therefore reduced, by the so called activation loss. This loss mechanism shapes the very left end of the course of Figure 2.3, highlighted in green colour. At larger electrical current density levels, that loss can be considered to have reached a small share in comparison to the ohmic losses. The fuel cell's behaviour reflects the expected behaviour of a resistor and therefore follows Ohm's law. The cell terminal voltage decreases almost linearly in the yellow marked middle load regime. Approaching the maximum achievable current density at the right end of the polarisation curve, the transportation losses become more and more important. In the blue shaded high load region, reactant and product flow rates, as well as diffusion rates, mainly determine the observed additional reduction in output voltage [24].

A satisfactory mathematical approximation of the observed terminal voltage V of a fuel cell can be made with Equation 2.2. The cell potential V equals the theoretically reached

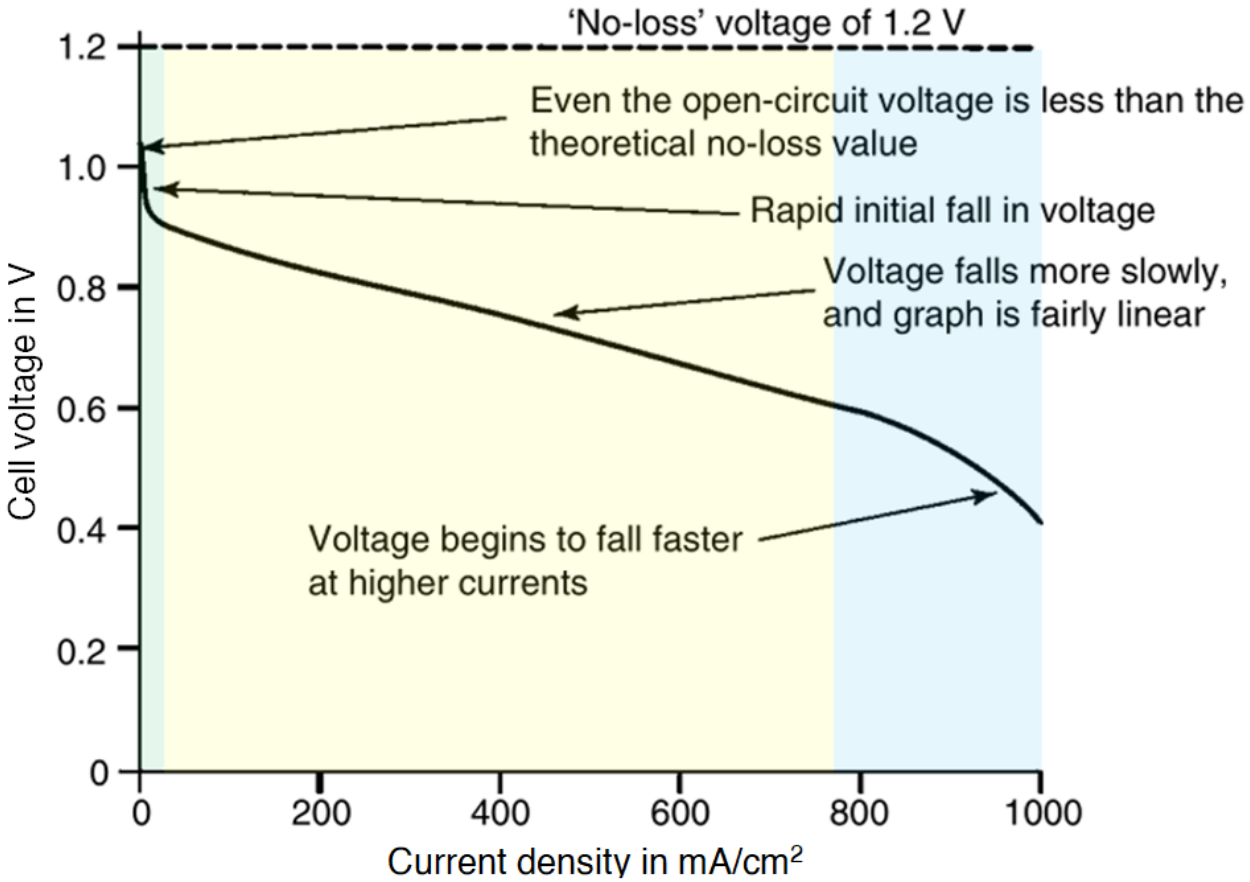

Figure 2.3: Generic polarisation curve of a low temperature fuel cell with highlighted loss regimes [2]. (modified representation)

cell potential E under the specific operating conditions minus the voltage losses, corresponding to the respective electrical load. Activation loss $V_{act\ loss}$, ohmic loss $V_{ohmic\ loss}$, and the transportation loss $V_{transp\ loss}$ are each represented by one term in Equation 2.2 [24].

$$V = E - V_{act\ loss} - V_{ohmic\ loss} - V_{transp\ loss} \tag{2.2}$$

It should be stated, that the actual behaviour of a fuel cell is greatly depending on the operating conditions. Pressure and temperature, as well as reactants concentrations, affect the electrochemical reactions that take place. The Nernst-equation [2] describes these phenomena, and expresses the dependency of the reversible cell voltage on the cell temperature and activity of reactants. One conclusion of the Nernst-equation is, that operating a fuel cell at higher pressure and temperature has a positive effect on cell potential. In turn, a higher cell potential means more output power and higher efficiency for a given cell [2, 24].

[2] Please see [2] for detailed information.

Gas Processing

The Nernst-equation shows mathematically, that fuel cells work better if they are operated at pressure levels raised above ambient conditions. On the anode side, the H_2 pressure control valve is used to determine the gas flow towards the fuel cell stack. Recirculation of the anode gas is carried out to obtain desirable flow conditions and evenly distributed reactant concentration in the anode compartment, and to effectively manage the water household within the stack [2].

Excess water is removed by the andode gas flow from the electrochemical active cell regions, and it is captured in a water trap. Other impurities, due to permeation or leakages, are purged out of the anode. This way, uniform operation conditions are ensured all across the anode side of the cell surface [2, 10]. To carry out the anode gas ecirculation, system designs which use an electrically driven recirculation pump or an ejector pump were layed out. The latter one being much more simple designed, as there are no moving parts involved. A drawback to ejector pump systems is, that the recirculation gas flow is enhanced only if fresh hydrogen is fed to the cell [2].

On the cathode side, an air compressor is used to regulate the pressure and to keep the distribution of the oxygen concentration equal over the cell surface. These compressors have to meet strict requirements in terms of air purity and controllability. The PEMFC is highly sensitive to impurities in both of its gas paths, hence lubricant free bearings have to be used [2, 14, 24]. Conceivable compressor types are the roots compressor, radial compressor, axial compressor and screw compressor, to name a few. In modern FCHEV applications mainly radial compressors are used for several reasons. They can be designed to suit the demands of a fuel cell system very well in terms of flow rates and pressure ratios. They are well investigated in turbochargers for combustion engines and induce only moderate production costs [14, 26]. Critical operation phases are always encountered during start-up and shut down of the compressor, as contact friction occurs between moving and resting parts.

Air compressors, and recirculation and coolant pumps have to be taken into account for the net FCS power output, as their energy demand is significant. Their consumed power greatly affects the overall FCS efficiency. Particularly in low load regions, i.e. minimum compressor speeds cause the system efficiency to reach its lowest values [2, 11, 13, 14, 16]. For reference see Figure 3.8 and 4.6, where the power demand of each auxiliary drive is plotted over the corresponding stack current density or stack power, and Figure 3.9 and 4.4, showing the stack's and overall system's efficiency.

A way to reduce the lost energy share is to recover part of the exhaust gas enthalpy by a turbine, in a similar way to a conventional turbocharger for internal combustion engines. The Mercedes GLC F-Cell, for example, uses an electrically assisted turbocharger. There exists an optimum air pressure level for the highest overall system efficiency. Output power characteristics of a fuel cell stack and the overall fuel cell system, with and without exhaust gas energy recovery, are shown in Figure 2.4 [14].

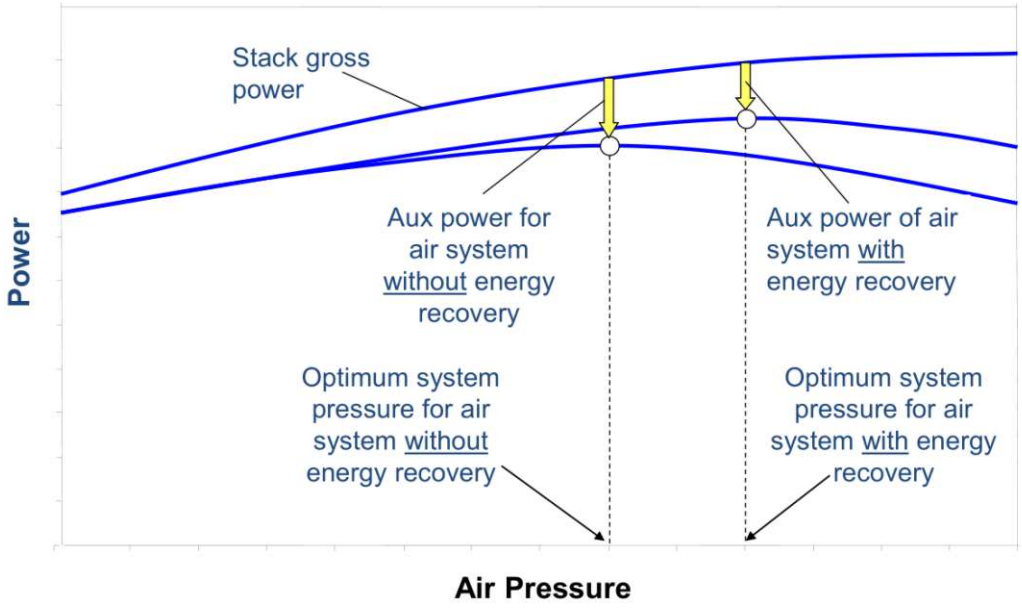

Figure 2.4: Generic FC stack output power characteristic (top curve) over various gas pressure levels. System output power course with (middle curve) and without (bottom curve) exhaust gas energy recovery [14].

Water management is a crucial topic for overall cell performance and its degradation behaviour. Besides for raising the working pressure of the fuel cell stack, air compressors are used for humidity management. The cathode gas flow transports away arising water vapour and liquid water from the active cell areas, so that fresh oxygen is there provided for the electrochemical reaction. Most vehicle models use a dedicated humidifier, to condition the stack's intake air [2, 14, 27].

The Toyota Mirai I and Mirai II are currently the only commercially available vehicle models, where the humidifier is eliminated by a self humidifying fuel cell stack. That is achieved by improvements of the anode and cathode flow fields, which are of high importance for the overall cell performance, as they have to provide homogenous operating conditions for each MEA across its whole cell surface [25, 26].

2.3 Fuel Cell Degradation

Fuel cells lose part of their original performance due to degradation. For a given current density, a degraded cell has a lower electrode potential, compared to a new cell [28–32]. The operating performance under steady-state and transient conditions deteriorates throughout the service life. There are various ways of measuring and evaluating the fuel cell's degradation rate and also to define the EoL. The EoL-criterion used in this work is defined as a cell potential loss of 10 % at a representative steady-state load point, according to [1, 29].

The fuel cell's electrochemically active areas are only the border regions, where catalyst particles and the electrolytic membrane are in contact. As energy conversion only takes place in those regions, it is generally opted to maximise that active surface to reach high power density and high efficiency. Gas diffusion layers are used to make the active surface accessible for the working reactants. Those diffusion layers have to be electrically conductive and highly porous, so that gas and product water can pass through them easily. Using fine structures in the design process therefore yields cells with minimum catalyst material usage, and a high specific power output [2, 24, 26].

In principle, all components within a fuel cell stack are suspect to degradation at some degree. The following section should give brief information on the known major degradation mechanisms and their impact on the different components. Furthermore, measures for mitigation of these mechanisms are presented.

2.3.1 Mechanical Degradation

All parts of a fuel cell stack are exposed to mechanical stress to some extent. Uneven distribution of heat causes uneven moisture contents and therefore shrinking of the membranes in locally dry areas. Cycling of shrinkage and expansion during the lifetime of a stack leads to pinholes or cracks in the membranes, and therefore enables gas crossover between anode and cathode gas [2, 33]. That not only causes direct fuel loss of unused hydrogen, but also enables oxygen and nitrogen to reach the anode. Nitrogen at the anode is not harmful for the materials and structure, but it dilutes the anode gas and therefore lowers the power output. Oxygen on the other hand, enables harmful carbon corrosion, which is described in detail in section 2.3.3. Local hot spots arise from rapidly increasing the load of the fuel cell stack and also from the start-up procedure. Therefore minimising the load fluctuations during operation and reducing the number of start-up and shut-down cycles is an effective way to reduce the mechanical degradation a fuel cell is exposed to.

2.3.2 Catalyst Degradation

Catalyst layers on the anode and the cathode of a fuel cell are used to lower the activation voltage loss, which is mentioned in section 2.2.1, and therefore increase the cell's efficiency. Modern catalyst compositions use fine particles from platinum or platinum-alloys, which are applied to carbon substrates. Generally, smaller particles yield a higher electrochemically active surface than bigger ones, for a given catalyst material mass. That would theoretically make the smallest manufacturable particles feasible, as the fuel cell performance directly depends on the size of the electrochemically active area. The degradation of catalyst particles however acts contrary, it proceeds faster with smaller particles and vice versa [34, 35].

During fuel cell operation, platinum is able to move within the MEA via ions and also by an insufficient interaction with the supporting carbon. Besides the macroscopic movement and then sintering together of small particles, two more mechanisms cause the loss of platinum from the electrochemically active surface areas for the fuel cell reaction, see Equation 2.1 [2, 34, 36].

On the one hand, dissolution of platinum into ions is favoured for particles with comparably high surface energy (depending on size and geometry of the particle) and correlated platinum ion equilibrium concentration around them. That process of disappearing of small particles and growth of bigger size catalyst particles is known as Ostwald ripening. On the other hand, platinum is also dissolved by reduction of platinum oxides, which are irreversibly formed and reduced through load cycling of the cell. Besides the growth of large particles, a sink for the dissolved platinum is the deposition inside the membrane. A so called platinum band is precipitated where the formerly movable platinum ions react with hydrogen coming from the anode. The result is a formation of immobile platinum particles beneath the interface of the membrane and the anode catalyst layer, which is not electrically connected to a catalyst layer [34, 36].

During the operation of a PEMFC, the growth of catalyst particles in the catalyst layer and the emerging platinum band in the membrane cause an additional cell potential loss due to the reduced size of electrochemically active surface area. The platinum band enables the direct catalytic combustion of hydrogen and oxygen, and therefore increases fuel loss. Experimental quantification of degradation of a fuel cell is a difficult task. Commonly used accelerated stress test procedures, which use a square wave load, do not degrade the catalyst the same way as real operation does. Therefore research for more appropriated test cycles is needed [36].

It has to be mentioned, that platinum catalysts are also vulnerable to intoxication with contaminants from the fuel or ambient air. The molecules of carbon monoxide (CO), as well as hydrogen sulphide (H_2S) and ammonia (NH_3) have a polar structure and therefore have to be considered dangerous for platinum catalysts. Although slight catalyst poisoning can be reversible, the before mentioned compounds have to be kept at very low levels for normal operation of the fuel cell [24].

2.3.3 Corrosion

The highly acidic environment in a fuel cell demands materials with very good corrosion resistance. A surrounding of pH 2 - 3 at temperatures around 70 °C applies stress on metals and organic materials, especially on the anode gas compartment parts [24].

Corroded metal parts, such as bipolar plates, would experience a decrease of conductivity and release metallic ions to the MEA. That in turn leads to a inactivation of the membrane's sulphonic acid group, and therefore to a reduced conductivity for hydrogen protons [33]. Carbon from the catalyst support is also prone to corrode during operation and especially during start-up, if hydrogen and oxygen are evident on the cell's anode.

Oxygen could permeate through the membrane from the cathode to the anode side during a shut-off period. At the following start-up, freshly applied hydrogen enters the anode and a hydrogen - oxygen front is formed. Because the protons experience much higher resistance travelling in plane of the membrane than trough it, that leads to a hydrogen - air fuel cell short circuited to an air - air electrolysis cell, see Figure 2.5. The cell potential rises until carbon oxidation starts to take place, and it runs until all oxygen is consumed or removed from the anode. The corrosion of the catalyst carbon support in turn leads to a loss of electrochemically active surface area and potential loss of catalyst material. Carbon also corrodes in areas, which are locally starved from hydrogen. This could happen during operation, if liquid water blocks the hydrogen from accessing the catalyst [34].

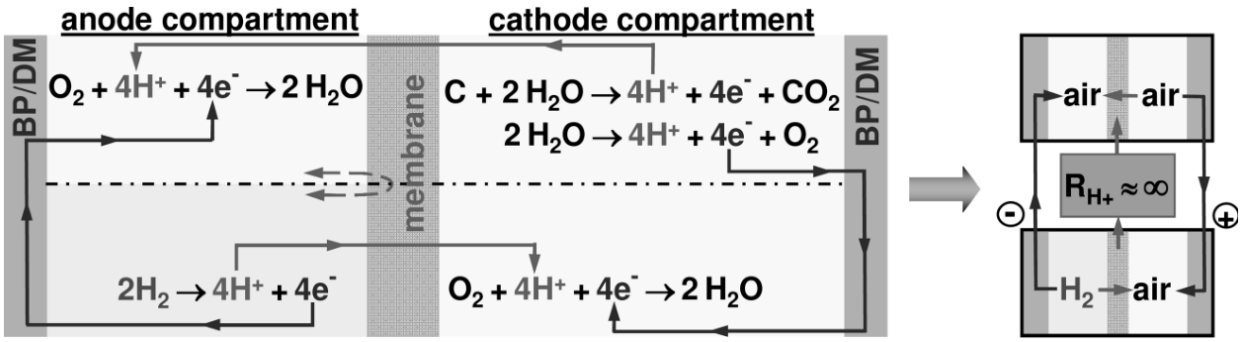

Figure 2.5: Simultaneous evidence of spatially separated hydrogen and oxygen at the anode causes carbon corrosion [34].

A big contribution to carbon corrosion is accounted to start-stop cycling of a fuel cell, orders of magnitude higher than corrosion during operation [37]. Important measures to mitigate the degradation of the catalyst support are applying hydrogen to the anode even during shut-off-mode, and quickly purging of the anode during start-up. Also the water management during the operation of the fuel cell takes on an important role in mitigating carbon corrosion [34].

2.4 Energy Management Strategies

The on-board rechargeable energy storage of the vehicle's serial hybrid powertrain structure enables special operation modes. On the one hand, the electrical machine and its controller can handle bi-directional power flow, so that part of the vehicle's kinetic energy during deceleration can be recovered. On the other hand, operating conditions for the main power source can be altered to the most efficient overall system operation, by using the secondary power source to buffer transient loads. An energy management strategy, also called vehicle control strategy in the literature, operates and decides about the power flows within the system [6]. Major objectives for such a strategy in a FCHEV could be the minimisation of one or more of the following objectives.

- Fuel consumption
- Fuel cell stack degradation
- HV-battery degradation
- Overall vehicle running costs
- ...

These in some way contrary individual targets are formulated into an overall objective function, which is processed by computerised algorithms. Approaching the minimum fuel consumption does in turn “cost” somewhat higher fuel cell stack degradation, so the process of optimising the EMS inherently invokes a trade-off to be made between the distinctive objectives. The mathematical background of an objective function might be simply a weighted sum of all considered individual performance indices, or might be even a set of functions to be applied on the results to retrieve an overall performance indicator. The objective function could also be interpreted as a cost function, which sums the costs arising from the distance the vehicle travelled. What else has to be considered for an EMS is the ability to be computed in real time, requirements on vehicle dynamics and robustness in differing driving conditions [5].

As mentioned in section 2.1, a serial hybrid vehicle is able to obtain the driver-demanded traction power from two separate energy sources and energy converters. The power split between the fuel cell stack and the high voltage battery is determined by the EMS. Depending on the logic behind the control functions, these strategies can be put into different categories, see Figure 2.6. Each approach has its own benefits and drawbacks, which are briefly highlighted in the following sections. At the end of this chapter, a strategy type will be chosen for the simulation model used in this work.

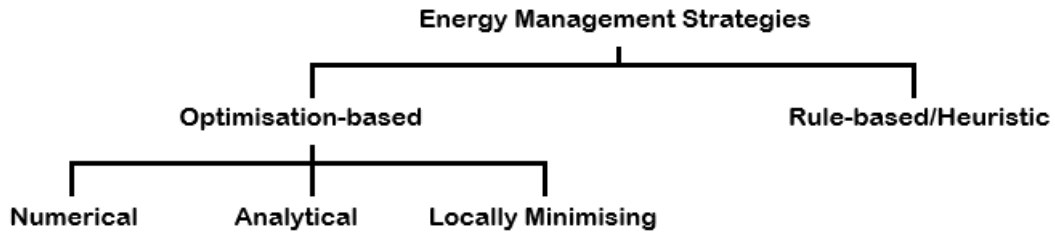

Figure 2.6: Categorisation of energy management strategies due to their working principle [38]. (modified representation)

Optimisation-based Strategies

The decisions of optimisation based energy management strategies about the applicable load to each available power source are derived via optimisation processes. As stated above, the EMS has to minimise the applied objective function result, with respect to

local boundary conditions. These are usually the charge sustaining of the HV-battery and power limitations of the electrical machine, the fuel cell stack and the HV-battery [38].

It has to be distinguished between a globally reached minimum of the objective function, or a local minimum. The global minimum is the absolute lowest possible total cost, for the vehicle running a certain test driving cycle. Per definition, the numerical and the analytical solution deliver both the global minimum of the objective function, within the limits of discretisation numerical tolerances. Numerically and analytically solved optimisation problems require high computational power, and demand knowledge of the whole driving profile in advance. They might not be directly applicable under realistic driving conditions, but their results can be used as benchmarks for testing of alternative strategies. One well known example of an analytical method is the Pontryagin's minimum principle, wehereas the dynamic programming is the widest known numerical method [38].

Locally minimising strategies do not necessarily find the global minimum, they might just find a local minimum of the cost function. But as these approaches only consider causal correlations of operation conditions at a given time, they are real-time capable for automotive applications. One well known example is the equivalent consumption minimisation strategy, which was first presented in [39]. As its name suggests, the power split between the two vehicle's power sources is chosen regarding an equivalent fuel consumption factor for the battery power share. The vehicle controller aims at each time step to minimise the overall fuel consumption, or cost, by choosing the power split with the lowest overall cost. An extension makes it equivalent to the Pontryagin's minimum principle, therefore the equivalent consumption minimisation strategy is also referred to as the real-time implementation of the Pontryagin's minimum principle [38].

Rule-based Strategies

This type of an energy management strategy performs its measures due to predefined rules and criteria for their input variables. In the simplest case, heuristically engineered and intuition based state switching rules are implemented. Other approaches are known to use fuzzy logic, or consist of rules, derived from optimisation processes. They are generally easily implementable for real driving applications, due to their plain nature [38].

For a given driving cycle and energy management strategy function set, the values of the switching parameters can be optimised to reach the minimum objective function value, or overall running cost. The resulting set of parameter values is though not necessarily useful for a different driving cycle. The robustness in different driving cycles of such a rule based solution greatly depends on the effort that went into it [38].

An overview of the advantages and disadvantages of the aforementioned strategy types can be gathered from Table 2.3, their performance in different categories is listed there.

Table 2.3: Rating of EMS types for a selection of requirements.

Strategy type	Numerical/Analytical	Locally minimising	Rule based
Quality of results	+ +	+	-
Real world applicability	+	+	+ +
Implementation effort vs. benefit for this work	- -	-	+ +

Choosen Strategy Type for this Work

A rule based strategy with parameters to be numerically optimised is chosen to be implemented in the vehicle model. The ease of implementation and low computational effort outweigh the drawbacks of that choice, as the main focus lies on a qualitative assessment of potential fuel cell degradation mitigation while fuel efficiency should be preserved. Possible gains, which could be reached with a more sophisticated EMS and more detailed simulation models are in contrast to the scope of this work. Minimising the fuel consumption and fuel cell stack degradation are chosen to be the main objectives of the strategy. Other requirements, like the system's robustness in realistic driving conditions and battery degradation should be considered for a production car as well, but that is beyond the scope of this work.

3 Methodology

A simulation model of an upper middle-class FCHEV is developed and validated in the ADAC ECO Test cycle, with the first generation Toyota Mirai being the reference. The fuel cell system core component models are created with data from other measurements, gathered on the IFA/TU Wien Fuel Cell test stand. The simulation model incorporates a data driven fuel cell degradation model, which is derived from a literature review. Numerical optimisation of the developed EMS is carried out to qualitatively point out possible gains in FC lifetime while maintaining high fuel economy in the WLTC-3b. The trade-off behaviour between minimum possible fuel consumption and minimum possible fuel cell degradation is assessed via the found Pareto front. A major simplification for these investigations is the use of quasi static simulation models. It is allowed to do so, because the result's accuracy is sufficient for energy management researches [40]. The model structure is built with a forward approach, which depicts information- and power-flows close to a real vehicle being driven [38, 40].

Figure 3.1 shows the schematic representation of the implemented FCHEV simulation model. Its components are described in detail in the following sections.

3.1 Vehicle Model

Each of the used individual component models for the chassis, wheels and tyres, brakes, transmission and the electrical machine, describes its core phenomena in sufficient detail. All submodels together depict the complete electromechanical drivetrain of the vehicle.

The **electric machine** model, please find its core data in Table 3.1, uses a literature derived efficiency map [41]. Figure 3.2 shows the machine's motor/generator efficiency and its full load characteristic. In the implemented version of the efficiency map, a fixed motor inverter loss of 3 % is taken into account. Therefore no dedicated motor inverter model is used, as seen in Figure 3.1.

All transmission losses of the real vehicle are gathered into one single **transmission** model with a constant efficiency of 96%, its input shaft coupled to the electrical machine. On the output side of the transmission, a **final drive** model is used to split the torque to both front wheels equally, and its power loss is already covered in the transmission model. Each **wheel** model incorporates a deactivated tyre model, which would normally add rolling resistance to the vehicle. The wheels are modelled with a constant dynamic rolling radius of 334.15 mm. Attached to each wheel is a **brake** model, which for this

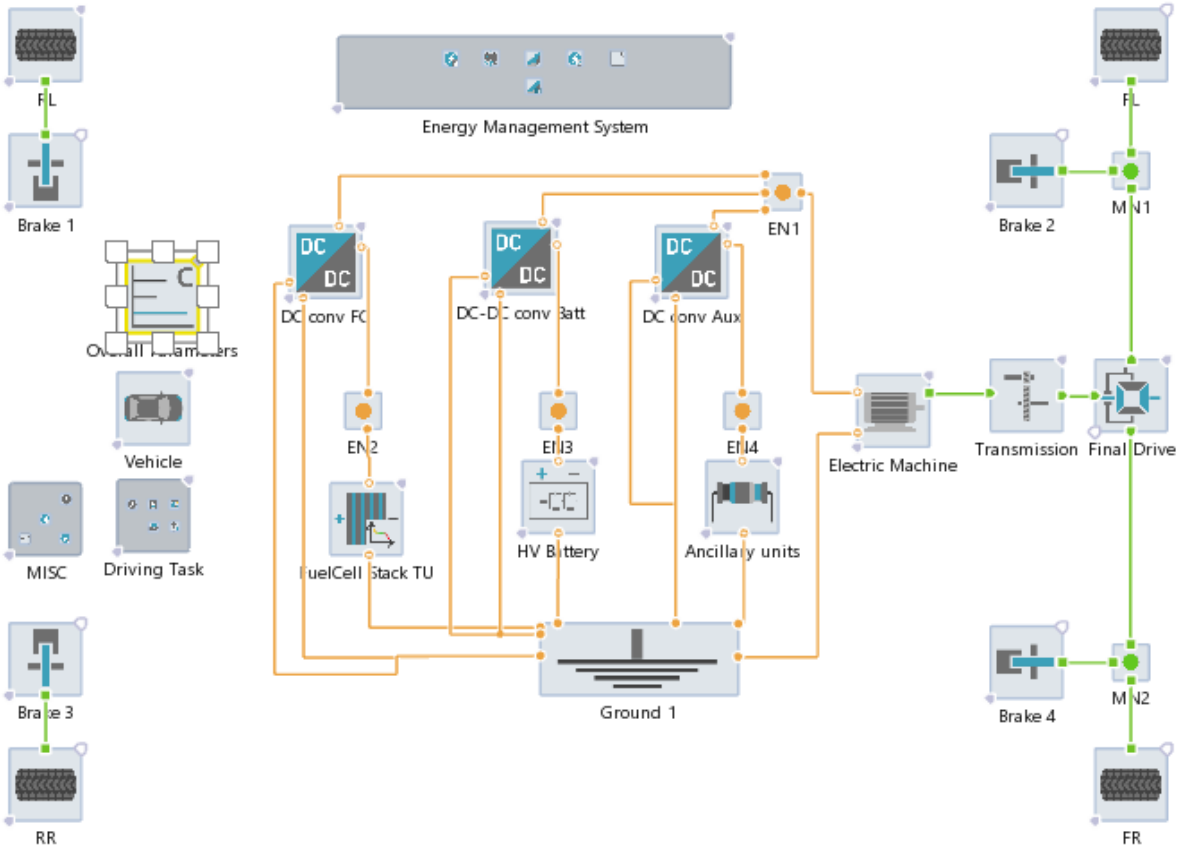

Figure 3.1: Graphic user interface representation of the implemented FCHEV model in AVL Cruise M.

investigation is merely a rotational mass. All these individual models include rotational masses, which contribute to the acceleration resistance of the vehicle. The vehicle's total static driving resistance and its curb weight of 1904.5 kg is known from measurements [22]. The function of the driving resistance force over the vehicle's speed [41] is implemented as a lookup table in the **chassis** model, and it is given in Figure 3.3.

Table 3.1: Key data of the electric machine [41].

Machine type	PMSM
Torque	+- 335 Nm
Power	+- 113 kW
Max. speed	12500 RPM

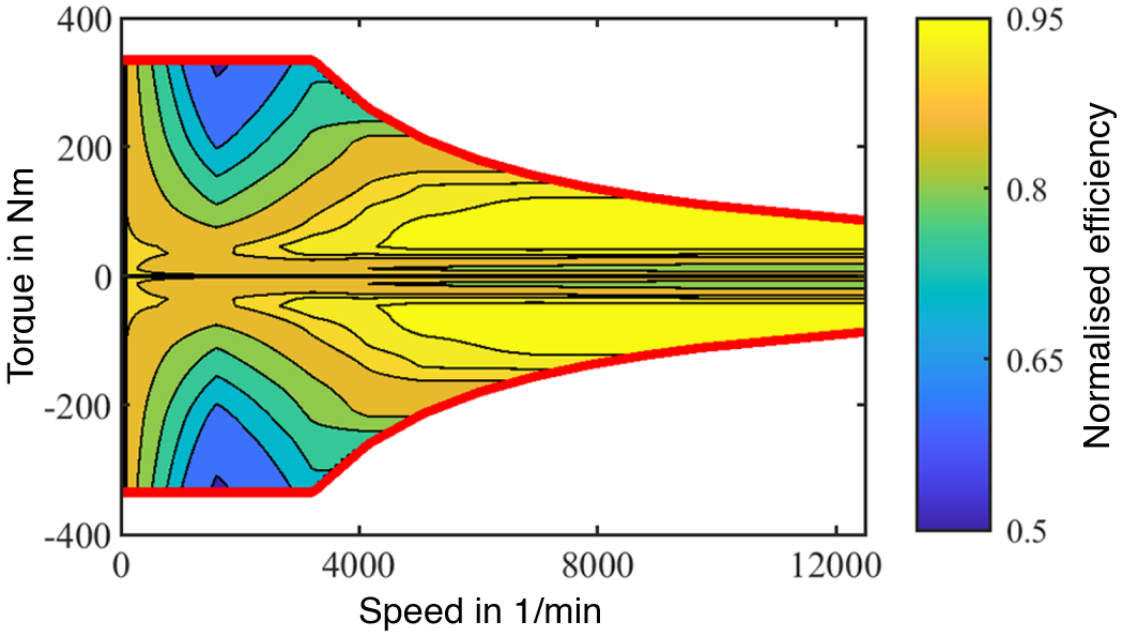

Figure 3.2: Efficiency map and full load characteristic of the electric machine [41].

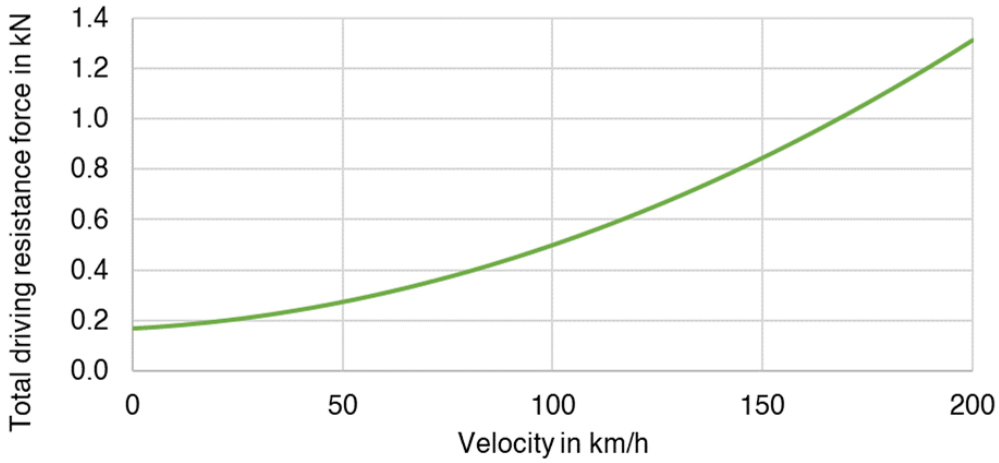

Figure 3.3: The chassis' velocity dependent resulting driving resistance force function.

This model setup is validated on the ADAC ECO Test cycle, of which measurements [22] of the real vehicle are available to the author. In a first step, the resulting velocity profile of the simulated vehicle is compared to that of the real vehicle. Figure 3.4 shows, that there are only minor deviations between the measured speed curve, the simulation result, and the target velocity profile.

Also the overall distance travelled of both exemplars are within a reasonable range. The measured vehicle travels a total of 48.6 m further, which is roughly 0.14 % of the whole distance driven. Therefore the conclusion is permitted, that the mechanical loading of the simulation model is similar to that of the real vehicle.

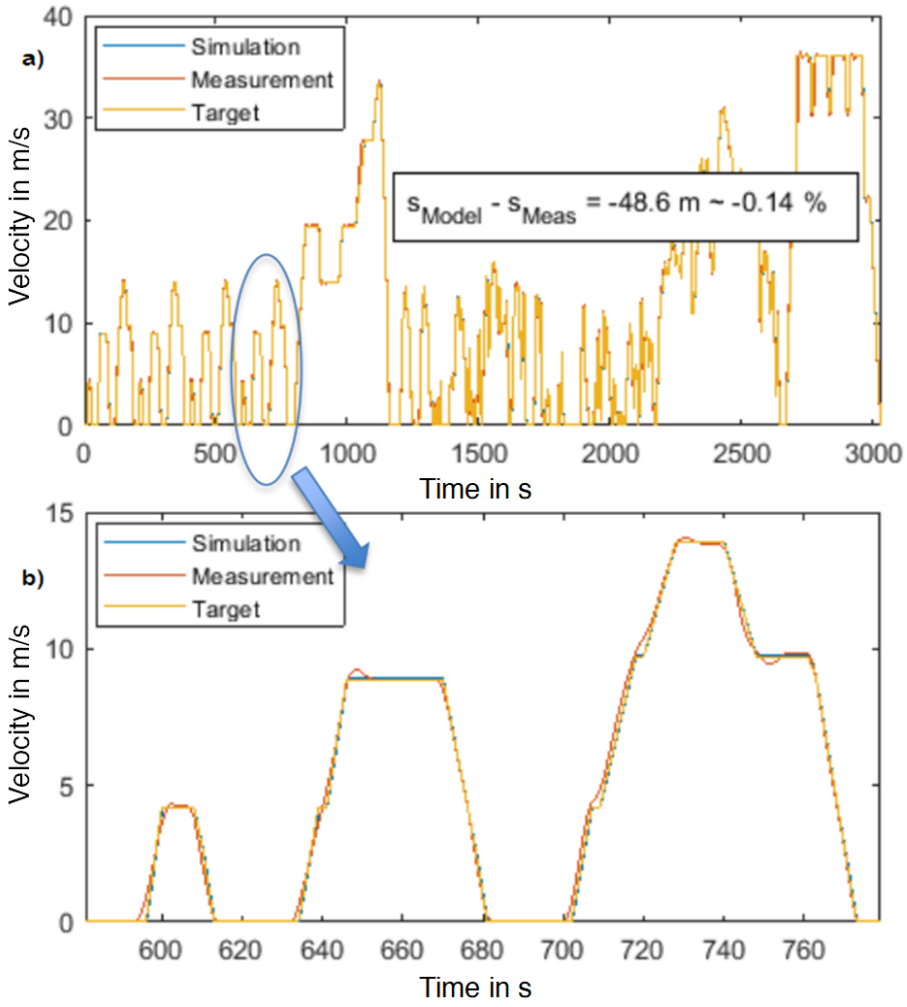

Figure 3.4: The velocity profile of the simulation result, the measurement [22], and the target of the ADAC ECO Test cycle.

The conformity of mechanical loads allows to compare the power consumption of the electrical machine as well. Figure 3.5 shows the close fit of the simulation results on their measured pendant. Furthermore, the model implemented energy recuperation yields a similar power trace, compared to the measurement.

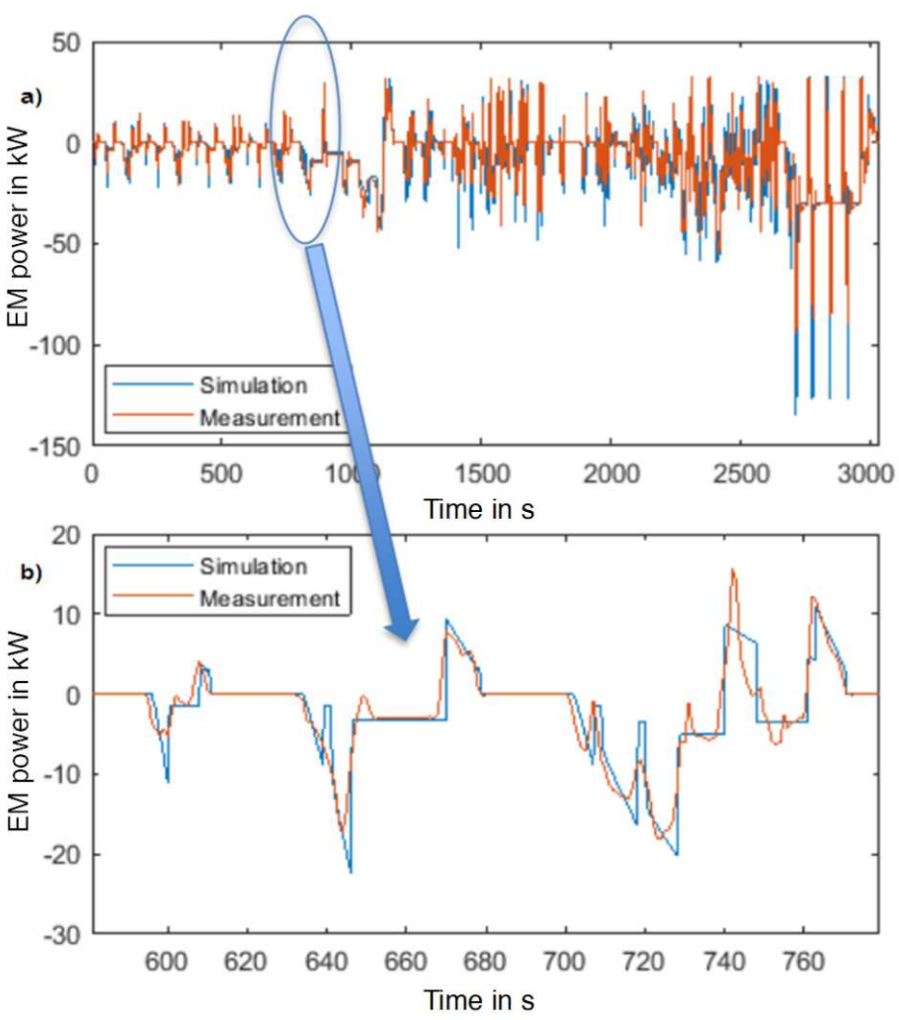

Figure 3.5: The comparison of the measured [22] and the simulated power demand of the vehicle's electrical machine in the ADAC ECO Test cycle.

The ADAC ECO Test cycle consists of the NEDC, which takes 1180 s to complete, followed by the CADC&BAB with another 1855 s of runtime. To check the model's accuracy in more detail, its energy demand in both parts of the ADAC ECO Test cycle is compared to the measurement. As seen in Figure 3.6, the model works evenly well under the wide range of driving conditions in both part test cycles. The model slightly underestimates the energy demand in the NEDC, at -1.9 %, and it overestimates the demand for 3.5 % in the CADC&BAB driving cycle. The overall energy consumption differs by only 1.6 %, with the simulation being more pessimistic than the measurement.

Thanks to the congruence of both, mechanical loading and electrical energy consumption, the model of the electromechanical vehicle can be taken as valid. With reasonable confidence, the simulation output of the model on a different test cycle, can be regarded to be similar to real measurements as well. That is the basis of the whole investigation series of this work, which is carried out on a different driving cycle, the WLTC-3b.

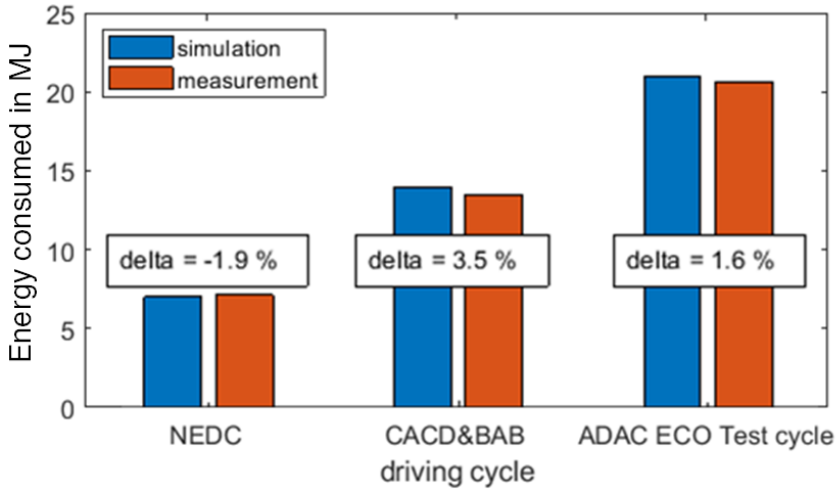

Figure 3.6: The simulation results and measured data [22] of the electrical machine's energy consumption.

3.2 High-Voltage Bus, Fuel Cell system, High-Voltage Battery and Cabin Consumers

The vehicle model's electrical components are embedded via equivalent circuit models, which are described in more detail in this section. All main consumers are electrically connected via a **high voltage bus** system, operating at 650 V. Three dedicated **DC/DC-converter** models, which are the interface between subsystems at different voltage levels, are contained in the vehicle model.

The fuel cell DC/DC-converter is used to step up the voltage of the stack's power output, it is a unidirectional current converter only. The HV-battery handles bi-directional power flow, therefore it's converter must handle that too. These two inverters are modelled with a fixed efficiency of 97 %.

The ancillary load model, which is described in more detail below, has its own unidirectional power converter. As it has to overcome a higher voltage difference than the other two converters, it is modelled to shift power with a constant efficiency of 92 %.

3.2.1 Fuel Cell Stack

On behalf of the TU Wien IFA, separate research series of a PEM fuel cell stack and its BoP components have been carried out on its fuel cell test stand.These measurements have been conducted on a stack with 96 cells and a maximum power of 28.1 kW, which is why an up-scaled version of that stack and its ancillaries is used in the FCHEV model. To meet the vehicle's power requirements, the fuel cell stack model has a five times multiple

cell count, compared to the measured example. See Table 3.2 for detailed information on the stack data.

Table 3.2: Key data of the fuel cell stack model in comparison to stack measured on the IFA FC test stand.

Item	Measurement	Model
Maximum power in kW	28.1	140.5
Number of cells in 1	96, serial	480, serial
Single cell surface in cm^2	409.5	409.5
Maximum current in A	500	500

In AVL Cruise M, there are different fuel cell models available. While other model types go into detail in terms of chemically, thermally and spatially resolution of an actual fuel cell, the “electrical model” of a fuel cell stack is most appropriate for this work. Hence here, the FC stack is mainly used to provide electrical power to the vehicle model. The FC stack model’s result is a time course of the cell voltages and current density during a simulation run. A newly developed fuel cell degradation model, proposed in section 3.3, extracts the cell voltage derating directly from the stacks’ power demand. Therefore neither physical, nor chemical simulations for the real degradation processes are needed.

The model setup of the fuel cell stack is carried out with the “Fuel Cell Parametrization Wizard”. This data input programme is used to convert results from the measurements into an electrical model of a fuel cell stack via inbuilt curve fitting. The user refined program’s suggestion of parameters yields a good reproduction of the input polarisation curve, which consists of six load points.

To verify the model’s performance, its polarisation curve is generated by performing a continuous current ramp from 0 to 500 A in 5000 s. So its current output is ramped up at a very low rate of 0.1 A / s, to meet the quasi-static measurement conditions of the real stack. Figure 3.7 shows the model input data (red asterisks) together with the model output (solid red line) and the relative error in absolute values (blue hollow dots) between the model output and the measurement.

In Figure 3.7, a 96 cell variant of the later used 480 cell stack is displayed, so that the corresponding load points of the measurement and the model result can directly be compared. Concluding it can be said, that the model reproduces the quasi static behaviour of the real stack with satisfying accuracy. The relative error at each measuring point is below +- 0.4 %. Furthermore, the environmental and operating conditions for the comparison are listed in Figure 3.7.

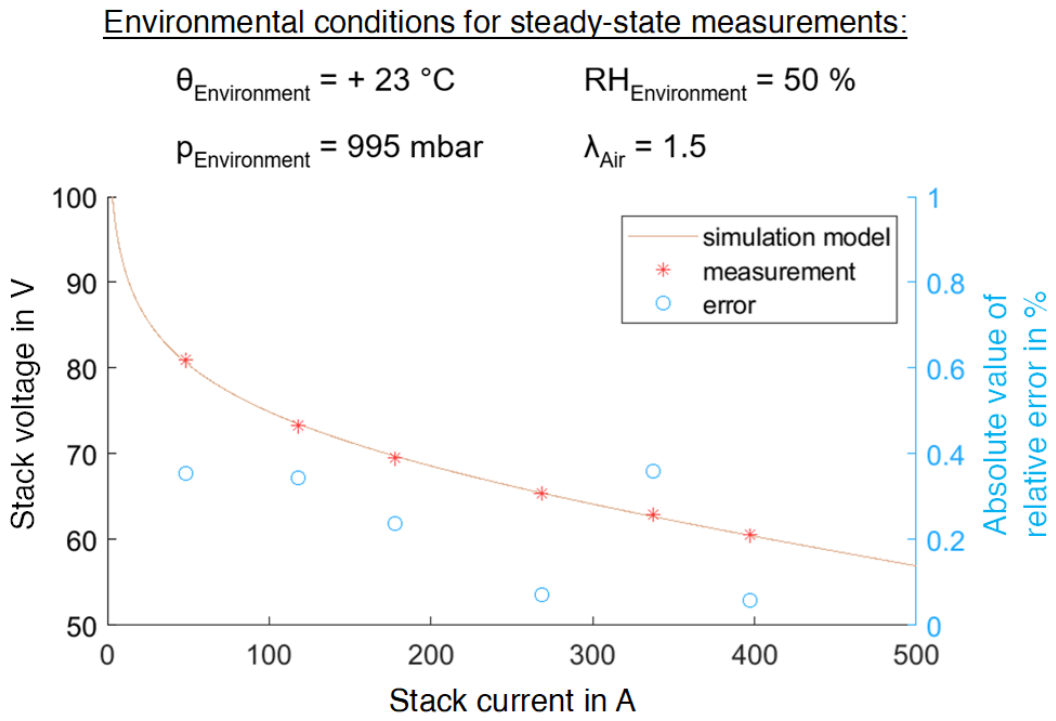

Figure 3.7: The resulting model polarisation curve, the error between a 96 cell stack model output and a measurement series on the IFA FC test stand.

3.2.2 Ancillaries of the Fuel Cell Stack and Cabin Consumers

The auxiliary drives of the modelled stack are a coolant pump, a hydrogen recirculation pump and an air compressor. Their respective power demand is known from the measurement series of the stack. All three ancillaries are similar in their systemic categorisation, each of them is an electrically driven fluid pump, and their operating voltage lies at 24 V DC. The measurement data consists of 6 points with ascending load, ranging from roughly 50 to 400 A of stack current. To implement these pumps in the simulation, the power demand of each of them is approximated via a quadratic polynomial function. These polynoms are used between 0 and 500 A stack current, with one exception. At current levels below 50 A, the power consumption of the compressor has reached its idle value. Therefore its power demand remains constant. The fitted modelling approach (lines) and the measurement data (circles)are shown in Figure 3.8.

For the energy management strategy only the sum of ancillary power consumption is of interest. The implementation into the vehicle model is made via a lookup table, and it is further described at the end of this section.

Fuel cells have relatively high efficiency on their own, over a wide range of load. However the overall fuel cell system efficiency, taking power loss of ancillaries into account, greatly depends on the applied load. In Figure 3.9, the stack efficiency and the overall system efficiency are plotted over the applied current density. The sweet spot, with the highest system efficiency, lies at around 155 mA / cm^2 and it reaches 56.9 %.

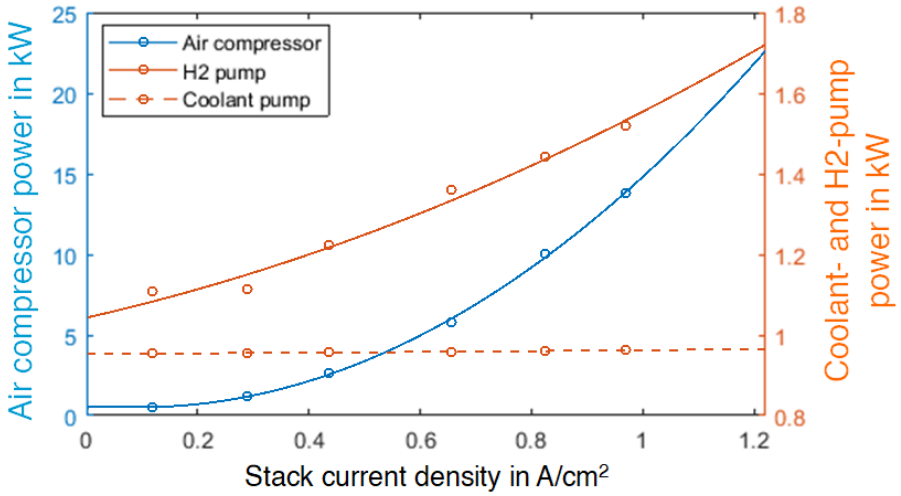

Figure 3.8: Modelled (lines) and measured (circles) power demand of the stack's ancillaries over the corresponding fuel cell load.

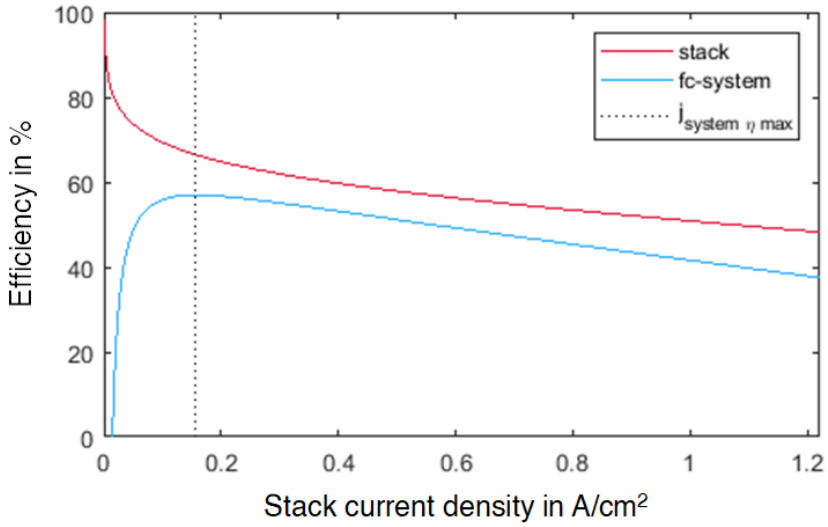

Figure 3.9: Model data: Fuel cell stack efficiency and overall fuel cell system efficiency over the stack load.

The vehicle's power sources also have to come up for the cabin consumer power demand. It is estimated that the cabin consumers draw a constant power of 700 W throughout a driving cycle, and it basically is a parasitic load to the high voltage system. The cabin consumers' power demand is added to the FC stack BoP components' power consumption, and that sum is implemented in a lookup table. Based on the FC stack load in each time step during a simulation run, an electrical substitute load demands the looked up power sum from the model's HV bus.

3.2.3 High Voltage Battery

The vehicle model uses a NiMH battery pack, with a nominal energy storage capacity of 1.6 kWh. It is made of 204 single cells, electrically connected in series. The power limits of the battery pack are in this work set to 30.8 kW for charging mode, and 18 kW for discharging mode. These limits are chosen in accordance with observations in measurement data from [16,22]. Detailled single cell data is derived from [42] and is used to parametrise the AVL Cruise M "battery" with the "Battery Parametrization Wizard". The inner resistance and the open circuit voltage of the resulting electrical equivalent model is shown in Figure 3.10 for a single cell.

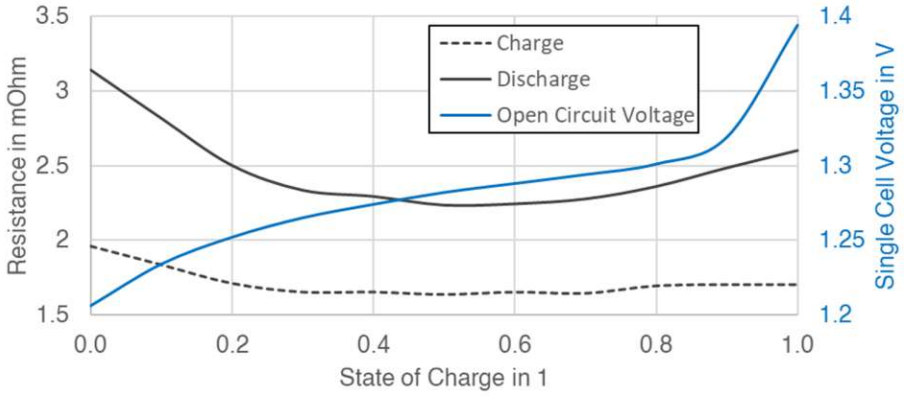

Figure 3.10: HV-battery model data: Single cell inner resistance and open circuit voltage.

3.3 Fuel Cell Degradation Model

Fuel cells degrade over their lifetime, and their output performance is greatly altered.

In section 2.3, an overview of the most dominant chemical and physical mechanisms for decreasing fuel cell performance during its lifetime is given. A highly sophisticated degradation modelling approach, in terms of causality and source of degradation, is made in [43]. The authors use a multiphysics fuel cell model to investigate catalyst degradation, caused by spatio-temporal variations in the flow fields.

This work however takes an abstract approach to this topic, similar to that in [29, 31]. Here only the impact of degradation on the cell performance at a reference load point is modelled. The amount of degradation is calculated from the load profile applied to the FC stack, and is expressed in μV of voltage loss of a single cell.

To define the EoL for a fuel cell, a convenient way is to choose a representative steady-state load point of the cell, i.e. a certain current output. The corresponding cell potential is the indicator for the actual health state. During the cell's use, the cell potential at this

current drawn is decreased. A commonly defined threshold value is 10 % of voltage loss at the respective load point, which is chosen for this work as well [1, 29].

The conclusion from the degradation mechanisms and their effects is, that the degradation progresses are heavily depending on operating parameters [28–30, 36, 44–46]. The categorisation of cell performance deterioration, found in the following sections, is based on the respective source of operation behaviour. The total modelled degradation arising from one simulation run, is the result of Equation 3.1:

$$v_{D,TOT} = v_{D,G} + v_{D,LC} + v_{D,SS} \tag{3.1}$$

Where $v_{D,TOT}$ is the overall voltage loss, while $v_{D,G}$, $v_{D,LC}$, and $v_{D,SS}$ are the voltage degradation sums of the galvanostatic, the load cycling, and the start-stop category respectively.

3.3.1 Galvanostatic Degradation

Operation of the fuel cell even at steady-state conditions causes degradation. This model category captures fuel cell performance loss, based on the occurring cell potential level and the time spent there. Therefore an assumption of a degradation function course is made, considering:

- Comparably high degradation rates at high cell potentials (idle condition), due to platinum dissolution and carbon corrosion.
- Wide region of low degradation rates at cell potentials from slightly above idle, up to medium load.
- Increased degradation rates at low cell potentials, or high loads. Caused by local starvation due to sub-optimal water management, various stress induced from hot spots.

Figure 3.11 shows the assumed function for the rate of cell potential loss, which is implemented in the degradation model. It shows a plausible course for the cell degradation rate between the blue points, which are derived from literature [3, 5, 31]. For easier handling in the implementation, the function is based on the actual cell current-density, which is higher for lower cell potentials and vice versa.

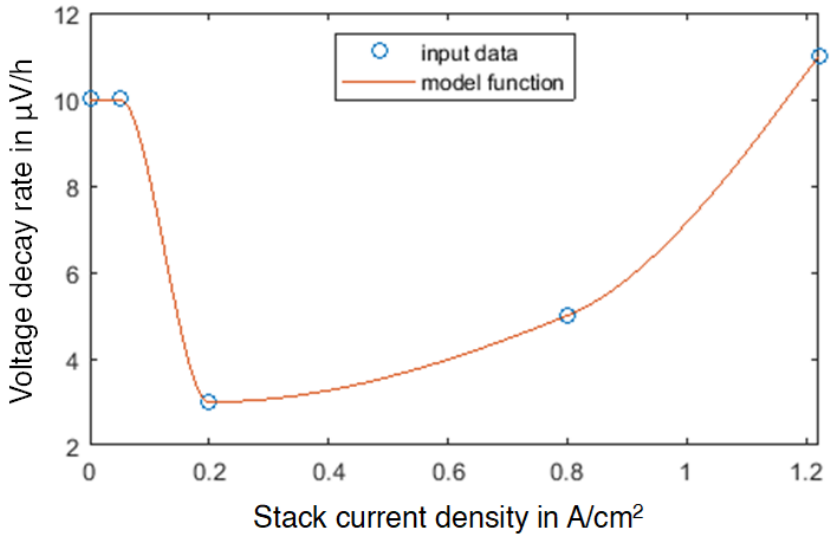

Figure 3.11: Model function of the galvanostatic fuel cell degradation rate over the stack load. Blue circles are model input data [3,5,31], the red line is model output.

This function is evaluated at the actual load point of each time step, and it is numerically integrated over the whole simulation run. It is therefore multiplied with the time increment size at each simulation step, according to Equation 3.2:

$$\Delta v_{D,G}|t = f_{gal}(j|t) \cdot \Delta t \tag{3.2}$$

Where $\Delta v_{D,G}|t$ is the incremental galvanostatic degradation, arising from the operation during the last simulation time step. The voltage decay rate function f_{gal} is evaluated at the occurring stack current density j at the actual simulation time t. The time step size between two computations is Δt.

The sum over all voltage loss increments from Equation 3.2 yields the total amount of the galvanostatic cell potential loss of one WLTC-3b driving cycle, and it is fed into Equation 3.1 as $v_{D,G}$.

3.3.2 Load Cycling Degradation

This category is meant to cover the degradation, emerging from changing the fuel cell load. The data found in literature is normalised on geometrical cell area and indicated by the blue circles in Figure 3.12. The function expresses the cell potential loss, which arises from changing the load of one cm^2 cell area for one kilowatt.

Input data is chosen from [28], with respect to other research results [3].

To obtain the representative occurring degradation from applying load changes, the absolute value of the geometric cell area related power change between two time steps is multiplied with the function value at the current stack load, according to Equation 3.3:

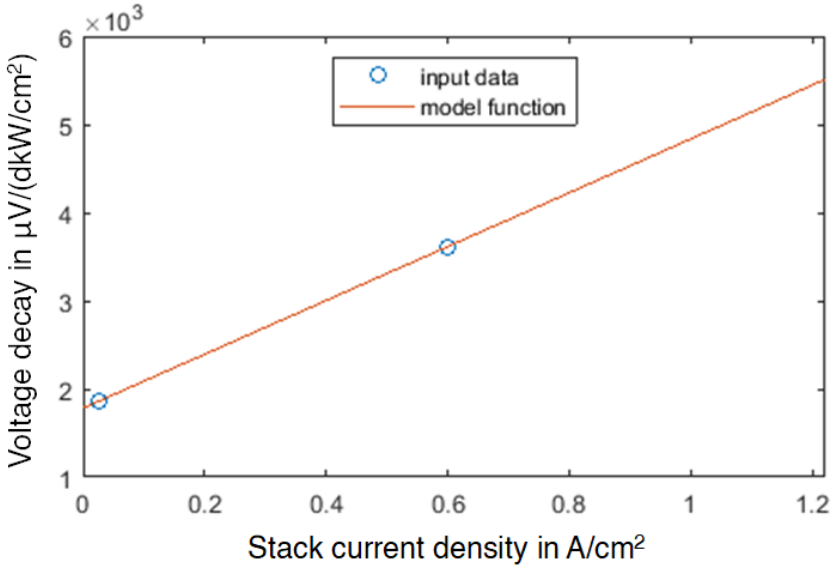

Figure 3.12: The implemented model function for cell voltage loss due to load cycling and the models' literature base data [28].

$$\Delta v_{D,LC}|t = f_{lc}(j|t) \cdot \frac{|\Delta P_{Stack}|}{n_{Cell} \cdot A_{Cell}} \tag{3.3}$$

Where $\Delta v_{D,LC}|t$ is the incremental load cycling degradation, arising from the load changing during the last simulation time step. The voltage decay function f_{lc} is evaluated at the occurring stack current density j at the actual simulation time t. ΔP_{Stack} is the applied load change to the FC stack during the last time step. The number of cells in the FC stack is n_{Cell}, and A_{Cell} is the geometric surface area of each cell.

At the end of a simulation run, the incremental load cycling degradation amounts are summed up to retrieve the overall degradation. This sum is fed into Equation 3.1 as $v_{D,LC}$.

3.3.3 Start-stop Degradation

As stated in section 2.3.2, a sequence of starting and stopping a fuel cell heavily stresses the catalyst layers. In fact it is source of one of the biggest parts of the overall degradation a fuel cell experiences in its lifetime. Observations found in literature note cell potential losses between 4 and 100 μV for a single start-stop-cycle. For this work's degradation model, the proposed average of these values is taken to map that effect at $v_{D,SS}$ = 25 μV per on-off sequence [3]. It is a simple additional term to the calculated degradation quantification value from the other two categories in Equation 3.1.

3.3.4 Implementation, Interpretation and Limitations of the Modelling Approach

The described degradation model is implemented into the simulation, as a data logging sequence only. It consists of an user defined “Compiled Function”, which accesses the galvanostatic and the load cycling degradation model in separate lookup tables. It calculates the representative cell degradation on the fly and it does not directly affect the energy management strategy.

The results are time profiles of the corresponding degradation category, gathered during the simulated test cycle. At the end of a simulation run, when the vehicle model has finished the driving cycle, the results are accessible for post-processing.

The result of the implemented model is a quantification of cell degradation for the distance travelled, expressed as loss of cell potential in μV at a reference load point. That reference load is chosen at 229 A for the implemented stack, corresponding to a current density of 0.559 A / cm^2, at which 0.7 V of cell potential are reached by a new cell. With the before defined threshold of 10 % voltage loss, 70 mV of cell potential loss represents the end-of-life criterion for this work.

This model uses only data of comparably fast degradation progression. That is achieved by the selection of the available data in literature. Besides that, other research findings point to the fact, that the progress of ageing processes is itself subject to change [28, 34, 35].

The author is aware of the fact, that this model lacks of an important component, which is the slope of the load change. It should be obvious, that if a fast load change is applied, steep gradients are expected to happen in the entire gas path domain of the fuel cell system, species concentrations, and heat fluxes. The other extreme is a quasi-static load change, where only negligible variations occur. From the knowledge base in section 2.3, it is concluded, that these two opposing cases induce different ageing mechanisms. So there is a need for further investigations to obtain a more comprehensive load cycling degradation model.

An advantage of the chosen degradation modelling approach is that only very little computational effort is needed. There is no need for further knowledge about the FC stack in terms of i.e. detailed geometry, or chemical formulation of its components. That makes the proposed tool efficient for qualitatively carried out assessments in the field of EMS development, which suits the overall intention of the presented work.

3.4 Energy Management Strategy

A rule based energy management strategy is implemented in the vehicle model. Its main functions are to maintain safe operation of all components via power limitation, and to minimise the overall vehicle running cost by fuel efficient and lifespan maximising operation

of the FCS. For this investigation, a boundary condition is to charge sustain the traction battery throughout the WLTC-3b driving cycle. Otherwise the optimisation for minimum fuel consumption would trim the EMS to use up as much energy from the battery as possible. That in turn would not be a sustainable way to operate the vehicle, as it would not be able to perform two or more driving tasks in a row with the same results.

The developed EMS consists of state switching components and internal memory. The implementation in AVL Cruise M is done via a “Compiled Function”, which is evaluated in “co-simulation” mode. That means, the code is executed once at the beginning of each time step. The strategie’s logic structure is given in Figure 3.13, the information flow is indicated by arrows.

As seen in Figure 3.13, the EMS is divided in two almost separate parts. The first part conducts a modification of the driver model’s output, it is located in the upper region of the diagram. The mechanical load signal for the EM is assembled from a positive torque demand (driver accelerates) and a negative torque demand (driver decelerates). The accelerator pedal position signal directly represents the applied positive torque demand for the EM.

In case the driver uses the brake pedal, energy recuperation is activated by applying a negative torque wish to the electrical machine. From the model parametrisation sections 3.1 and 3.2.3 it is known, that the maximum allowed charging power of the HV-battery is around 27 % of the maximum EM power. To lend similar vehicle acceleration and deceleration characteristics to the accelerator and brake pedal respectively, a chosen threshold value of 20 % brake pedal position represents maximum brake recuperation power. At brake pedal signals higher than that, also the mechanical brakes are actuated. This way, an useful regenerative braking regime is accessible for the driver model. The recuperation power limitation takes the maximum allowed HV-battery charging power and converter efficiencies into consideration.

Below vehicle speeds of 15 km / h, the amount of allowed recuperation power is ramped down to zero at a velocity of 8 km / h. At even slower speeds, the permission to recover brake energy is declined. That obtains operational stability in the regime of a low vehicle speed, and the car is held by its mechanical brakes in standstill situations.

The second part of the EMS calculates the vehicle’s overall power demand and then splits the load between its fuel cell system and HV-battery, considering the implemented strategy functions. As this investigation is about to optimise fuel consumption and fuel cell degradation, the chosen strategy rules are built modifiable by parameters. These rules are designed to make use of the hybrid powertrain structure, and to enable the fuel cell system’s operation close to its most efficient load region. Phlegmatisation and load shifting of the FC power output is also implemented to minimise the load-change induced FC degradation. Based on the vehicle’s power demand, the logic switches between three operation modes (decision block in the right hand bottom corner of Figure 3.13):

I. FC stack power off, HV-battery discharging mode: The HV-battery is the vehicle’s only power source.

II. FC stack power on & HV-battery discharging mode: Both FCS and HV-battery power the vehicle.

III. FC stack power on & HV-battery charging mode: The fuel cell stack provides power to propel the vehicle and the HV-battery is being charged.

These three different operation modes are taken into account by state switching variables in the layered power split computation sequence, centre right in Figure 3.13. In that sequence, a desired FCS power output is calculated from the vehicle's overall power demand. The target power output only takes fuel consumption and FC degradation rules into account, and it therefore has to be limited and/or changed by the second level calculation. This layer takes care of the HV-battery's electrical capabilities and possibly required charging power. In the third level, the FCS power output is once more adapted to securely fulfil the driver's power demand. It comes up for a probably emerged gap, induced by the second level HV-battery power limitation calculation.

3.4.1 Operational Objectives of the Strategy

The two major topics of this work are to minimise the operationally caused degradation of the fuel cell, and the minimisation of the fuel consumption of the given system. The following observations can be made from the FC degradation section 2.3 and the degradation model implemented literature data, they are therefore considered by the EMS:

- There is an operational region with comparably low galvanostatic voltage decay rates, which is at load levels above idle, up to medium loads.
- Low load levels present a favourable voltage loss operation range, due to lower load cycling degradation.
- Load fluctuation causes thermal and species inhomogeneities in the gas path, therefore steady-state operation yields lower amounts of stress on the FC stack.

From the fuel efficiency point of view, the EMS considers the following:

- There exists an optimum FC load. The efficiency optimum occurs between low and medium load, see Figure 3.9 for reference.
- From no load applied, the FCS efficiency rapidly rises to comparably high levels throughout a wide operational range.

A synergy between low and medium loads is that the FCS will make use of highly fuel efficient operation, while only low FC degradation rates are to expected. That is, coupled with a dedicated phlegmatisation function, also a means to reduce the load cycling degradation. A downside of phlegmatisation is, that the produced energy is passed through a longer efficiency chain until it is used. The multiple conversion of energy therefore will increase the overall fuel consumption. The detailed trade-off behaviour between minimised

fuel consumption and reduced FC degradation of the developed models and the EMS is pointed out with this investigation.

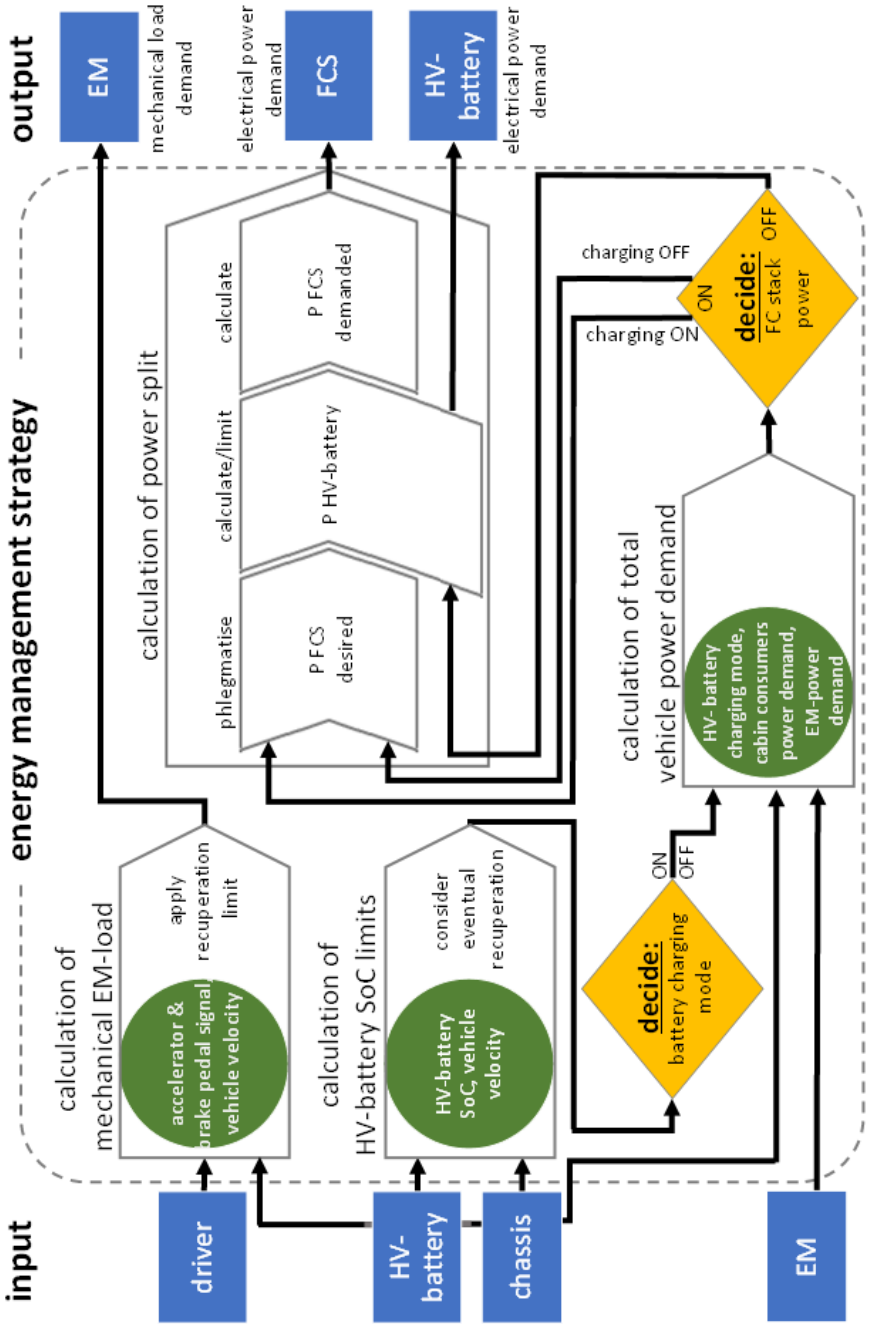

Figure 3.13: Logic structure and signal flows of the developed energy management strategy.

3.4.2 Strategy Rules in Detail

To enable the EMS's switching and calculating rules to adopt for high fuel efficiency and low degradation operation, they are designed with 9 individual parameters. The chosen optimisation algorithm varies them, to achieve the desired optimisation target. Detailed information about the optimisation workflow is found below, in section 3.5. Without emphasis due to the numbering in the following list, the EMS parameters (P_1 to P_9) are briefly described here:

- P_1 **Minimum fuel cell stack output power.** The fuel cell stack is only operated, if its demanded power output is higher than that threshold value. A hysteresis is applied, to prevent erratic switching in case of slightly fluctuating power demand.
- P_2 **Fixed power output within phlegmatisation band.** Whenever the calculated power demand for the fuel cell system is within a certain band, no load fluctuations are applied. The system is operated at the power level specified by P_2, see Figure 3.14 for reference. The idea is, to minimise load fluctuations to the fuel cell stack, and therefore reduce the accompanying degradation mechanisms.
- P_3 **Phlegmatisation band upper width.** This parameter determines how wide the phlegmatisation band reaches above the fixed power output level (P_2), see Figure 3.14.
- P_4 **Phlegmatisation band lower width.** The width of the phlegmatisation band below the fixed power output level (P_2) is described by this parameter, see Figure 3.14.
- P_5 **Phlegmatisation time window.** Further phlegmatisation is applied via computing the time-based average power demand. The time window parameter describes the length of the interval, for which the average power demand of the vehicle is calculated. This average value is intended to sustain the battery charge and to reduce load fluctuations applied to the fuel cell system.
- P_6 **Accepted usage of battery state of charge before recharging.** A threshold for the minimum HV-battery's state of charge is defined, with reference to the state of charge (SoC) of the starting point of the driving cycle. The EMS starts recharging, everytime the battery SoC falls below the here specified amount, see Figure 3.15. The minimum permissible SoC is lowered with increasing vehicle speed, as recovered energy from the following braking process restores part of the battery charge.
- P_7 **Amount of Energy being charged into the battery.** Once the EMS decides to recharge the battery, it runs the charging process until the here defined state of charge has been restored. In Figure 3.15 the blue spotted line indicates a charge sustaining operation on a whole driving cycle, which is the major function of P_6 and P_7.
- P_8 **Battery charging power factor.** This factor determines the actual charging power from the FCS, by scaling down the battery's maximum allowed charging power. During a charging phase, the EMS opts to draw a constant power level from the FCS

to charge the HV-battery. In case of high brake energy recovery amounts, the FCS output is ramped down to respect the battery's charging power limit. Figure 3.16 shows schematically the charging process without energy recovery, and moderate and strong energy recovery. Converter efficiencies are hinted at, but to clarify the charging function no other EMS feature is shown.

P_9 **Battery discharging power factor.** If the battery is not being charged, it is operated in discharging mode. The EMS demands a downscaled amount of the FCS power output from the battery. The battery output is limited in times of high FCS output to ensure safe operation, see Figure 3.17.

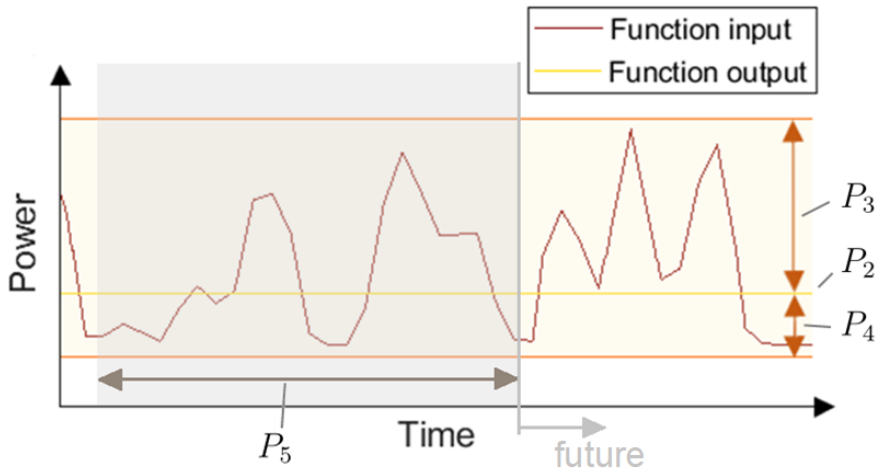

Figure 3.14: Schematic illustration: Phlegmatisation parameters 2, 3, 4, and 5.

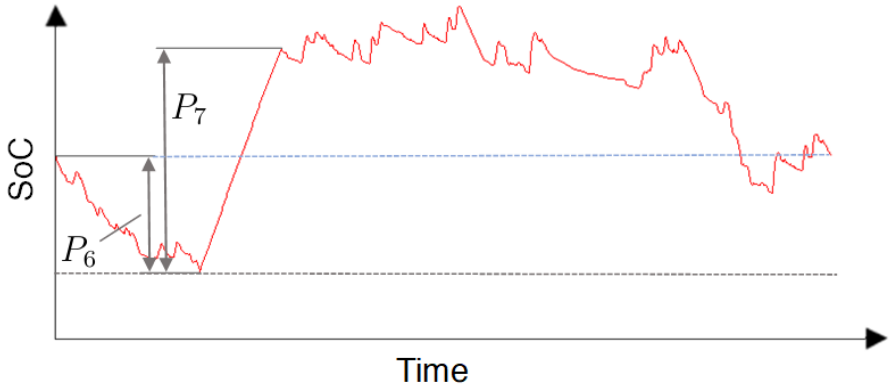

Figure 3.15: Schematic illustration: HV-battery recharge SoC minimum and recharge amount parameters 6 and 7.

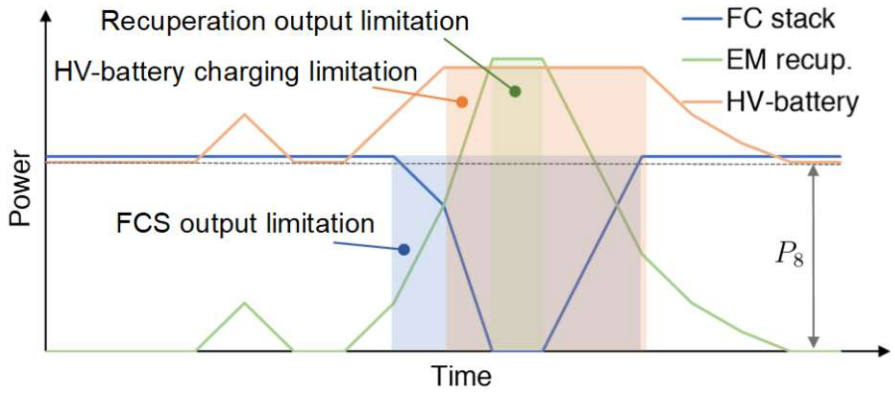

Figure 3.16: Schematic illustration: Power split with EMS in HV-battery charging mode and EM brake energy recovery, and parameter 8.

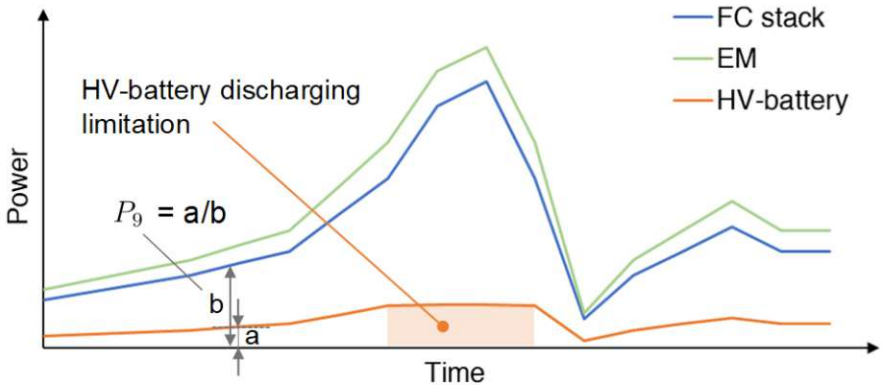

Figure 3.17: Schematic illustration: Power split with EMS in HV-battery discharging mode, and parameter 9.

3.5 Optimisation Workflow

The previous sections describe the setup and validity of the vehicle model. That yields the basis for the conducted investigations of the vehicle in the WLTC-3b driving cycle, which are described here. The fuel consumption and the fuel cell degradation are about to be minimised via variation of existing parameters.

The work flow of the optimisation process is depicted in Figure 3.18. The model is operated in the driving cycle and therefore produces results, consisting of time based flow rates and their integrated flow over the whole time interval. These results are stored to enable the optimisation process to be followed during the operation and also after the process has finished. Based on the objective function's result, changes are applied to the 9 EMS parameters (section 3.4.2) by the optimisation algorithm. Then new simulation runs are carried out with the model, which is equipped with the refined parameter values.

Figure 3.18: The work flow of a numerical optimisation process, heavily simplified.

In this work, the task of parameter optimisation is carried out by a python-script [3], which operates the simulation environment AVL Cruise M.

3.5.1 Optimisation Algorithm

In literature, there are several optimisation algorithms available to choose from. For this work, a differential evolution (DE) algorithm is chosen to perform the optimisation process. It is most appropriate, as it is able to find the global minimum of a function at reasonable computation efforts [47].

The DE algorithm is a type of genetic algorithms, which imitate a biological evolutionary process. A stochastically generated initial population yields a collection of results, where the most promising results are derived from the “fittest” individuals. These are allowed to be combined and to propagate, while the less fittest individuals are withdrawn. A certain amount mutation is applied on the fittest individuals before they are combined, and these combinations then represent the next generation of the investigated population [48].

There are different ways to define a convergence criterion for the found solutions, of which the “relative tolerance” is used here. The standard deviation of the all individual’s solutions can be interpreted as the population’s energy. The algorithm calculates the relative tolerance by norming the population’s energy on the mean value of the individual’s solutions. For this investigation, the relative tolerance abort criteria is set to 0.001, which is lower than the default value of 0.01. This means that solution convergence is defined in a way that all individuals have approximately the same objective function value. In other words, convergence is recognised if the population has only negligible energy. The aforementioned objective function assesses the overall performance of an individual, it is described in more detail in section 3.5.3.

An additional abort criterion for the process is the maximum iteration number, which defines the number of allowed solution generations to be formed by the algorithm. For this 9-dimensional investigation a limit of 5000 generations is chosen, to securely reach solution convergence before that limit is approached [49]. Figure 3.19 shows exemplarily the convergence behaviour of three equally set up optimisation queries. Each of them finds

[3] The original python-script and comprehensive support is kindly provided by Maximilian Haslinger, who is its author.

the same solution, but due to the stochastic formation of the initial generation, each query converges at a different rate.

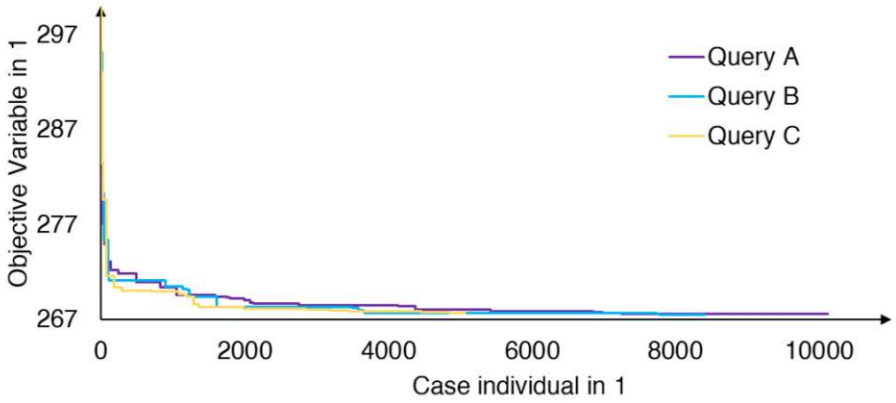

Figure 3.19: The convergence behaviour of three equally set up optimisation queries.

3.5.2 Trade-off Behaviour Investigation Approach

One focus of this work is to gain qualitatively assessed insights into the trade-off behaviour between fuel cell degradation mitigation and fuel consumption increase. The fundamental idea is to use the same EMS throughout this work and only to alter its parameters. To run the simulation model, each of the modifiable parameters needs to have an appropriated value assigned. Such a set of parameters is called “case”, and a simulation run of that case produces a corresponding result. To obtain a reference, on how the particular parameter value set performs, benchmark cases are searched for.

Two things are assured to obtain valid results for eventual cross referencing. Firstly, the driving task is carried out without violations of the demanded velocity profile. Secondly, the HV-battery is charge sustained throughout the driving cycle. The vehicle starts the driving cycle with a SoC of 60 %, and finishes it with slightly above 60 %. The actual fuel mass used for one cycle is therefore directly derived from the simulation results without further necessary computation or electricity equivalence calculations.

The first benchmark is retrieved from an optimisation process for minimum fuel consumption on the test cycle, using the full parameter space available. No fuel cell degradation is considered, so that the lowest possible fuel consumption for the given EMS structure is found. In this simulation series, a strong correlation between the minimum fuel cell stack power (parameter **1**, see section 3.4.2) and the fuel consumption is revealed. To greatly simplify the following optimisation processes, due to a higher content of feasible cases, the stack minimum output power is held constant. The resulting benchmark for minimum fuel consumption is referred to as $m_{H_2,b}$.

The second benchmark is the minimum fuel cell degradation case. As mentioned before, this optimisation job is performed with 8 parameters remaining. The voltage decay benchmark, in terms of least fuel cell degradation, is referred to as $v_{D,b}$.

To precisely point out the model behaviour between minimum fuel consumption and minimum fuel cell degradation, further optimisation runs are made. Therefore an objective function is developed, to merge both performance indices into one single variable value, see details in section 3.5.3. These further optimisation runs are made with different weighting of each performance index in the summing objective function. This way, it is assumed, all relevant non-dominated points between minimum fuel cell degradation and minimum fuel consumption are examined. Detailed information on the results is provided in chapter 4.

3.5.3 Objective Function

It is the nature of the DE algorithm, that the fitness of a case is only assessed by its objective function value resulting from the simulation run. The two performance indices, fuel consumption m_{H_2} in kg / cycle and fuel cell voltage decay v_D in μV / cycle, therefore have to be combined in a single objective function. Mathematical conditioning takes care of the different units and magnitudes of order of the two indices. The value of m_{H_2} is around the magnitude of $3 \cdot 10^{-1}$, whereas the value of v_D lies at around $6 \cdot 10^{1}$.

The chosen approach for the objective function is a weighted sum of conditioning functions of the initial objective variables, which yields a single dimension-less performance indicator. The objective variable's mathematical expression is given in Equation (3.4). Based on the two benchmark cases for minimum fuel consumption ($m_{H_2,b}$) and minimum FC degradation ($v_{D,b}$), the objective function assesses the performance of the actual case. The individual contributions to the summed up objective variable's value are weighted with a factor w .The weighting of each objective is therefore easily modifiable during the workflow, to precisely direct the algorithm to investigate in certain objective regions.

$$\begin{aligned} OV &= f\left(m_{H_2}\right) \cdot (1-w) \quad + f\left(v_D\right) \cdot w \\ &= \left(\frac{m_{H_2}}{m_{H_2,b}}\right)^6 \cdot (1-w) + \left(o + \frac{v_D}{v_{D,b}} \cdot k\right)^6 \cdot w \end{aligned} \tag{3.4}$$

Where OV is the objective variable, w the weight of fuel cell degradation, o a constant offset, and k a scaling factor.

The input variables m_{H_2} and v_D have different result intervals in the investigated solution area. The benchmark case for minimum fuel consumption uses only 3.55 % less fuel than the benchmark case for minimum fuel cell degradation, whereas up to 28 % of *mitigable* [4] fuel cell degradation is avoided in the corresponding benchmark case. To come up for that mismatch, the normalised degradation is scaled by the factor k and an offset o is applied. Equations 3.5 and 3.6 yield the respective parameter.

[4] The fuel cell system is started one time at the beginning of the driving cycle, which is why it contributes a constant additional term for all cases. It therefore is not mitigable.

$$k = \frac{m_{H_2,S}}{m_{H_2,b}} \cdot \frac{v_{D,b}}{v_{D,S}} = 0.12748 \tag{3.5}$$

$$o = 1 - k = 0.87252 \tag{3.6}$$

With $m_{H_2,S}$ being the consumed fuel mass of the degradation benchmark case, and $v_{D,S}$ being the FC degradation of the fuel consumption benchmark case.

The idea is to hereby obtain two harmonised dimension-less inputs to the objective function in Equation 3.4, with $f\left(m_{H_2}\right)$ and $f\left(v_D\right)$ having the same solution interval. The power of 6 is applied to the individual functions to amplify the objective variable's distinctiveness. This value is chosen to provide a sensible solution area to be investigated by the algorithm, while introduced numerical noise is kept small.

Figure 3.20 shows the objective variable's iso-lines for three different values for the weight w, resulting from a sweep test of both input variables of the objective function. Here, $v_{D|m}$ and $v_{D,\ b|m}$ represent the *mitigable* content of the total fuel cell degradation, to emphasise the range of possible improvements. Only the most feasible region of the solution space is shown, with the lower corners at an axis value of 1 representing the benchmark cases.

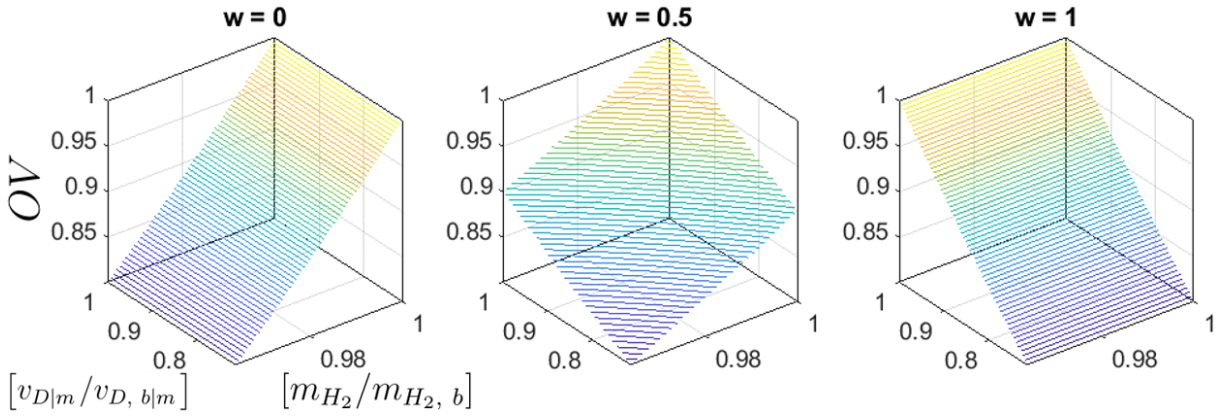

Figure 3.20: The objective variable's iso-lines in the most feasible solution space, for w = 0, 0.5, 1.

From Figure 3.20 it can be seen, that for i.e. w = 0, the value of $v_{D|m}$ does not affect the value of OV. That means no weight is applied to the fuel cell degradation. On the other hand, for w = 1, all weight is applied to the fuel cell degradation. The objective function value is therefore not changed, if m_{H_2} is changed. For w = 0.5, the iso-lines of OV are angled at 45 °. That means a lower fuel consumption is equally appealing to the algorithm as a reduction in fuel cell degradation. This experiment shows, that the objective function and its weighting function work as expected.

Reflections on the Optimisation Job

The optimisation workflow is executed efficiently and yields satisfactory results. A manually conducted design of experiments, with i.e. only 10 different parameter values for each parameter's domain, would here lead to 10^9 different parameter sets to be investigated. Then it still would be a lucky incident to find optimal parameter combinations.

To check and verify the DE algorithm's output, three optimisation queries are set up equally and are executed in parallel for each weight w in the objective function. One DE algorithm conducts an average of only around $7 \cdot 10^3$ simulation runs for each optimisation job, before the results reach convergence. The three data sets, retrieved from the three independent operations, show congruent trends. That is, why the results are finally pooled together.

In total, roughly $8 \cdot 10^4$ individual simulation runs are carried out. That is a great reduction of computational efforts, in comparison to a design of experiments.

4 Results and Discussion

Investigations for the mitigation of fuel cell degradation and fuel consumption reduction are carried out in the WLTC-3b driving cycle. The minimum possible fuel consumption, and the minimum possible fuel cell degradation, for the given combination of EMS/degradation-model/vehicle model are searched for via numerical optimisation. These two benchmark cases are used to measure the quality of all further retrieved results. The EMS's function parameters are precisely altered to maintain both fuel efficiency, and low degradation of the fuel cell stack. This way, the trade-off behaviour between the two partially contrary targets is elaborated and highlighted.

4.1 Benchmark Results and non dominated Points

4.1.1 Minimum Fuel Consumption Benchmark Case

For the search of the parameter set, which achieves the minimum attainable fuel consumption on the given simulation model combination, all 9 EMS-integrated parameters are used. See the parameter list in section 3.4.2 for reference. The optimisation run finds the lowest possible fuel consumption at 0.2674 kg of hydrogen, for one WLTC-3b driving cycle. That corresponds to a hydrogen mass of 1.15 kg used per 100 km distance travelled. For this case, the fuel cell degradation model calculates a representative voltage decay of 68.95 μV for one driving cycle. Expressed in operation time, that yields a voltage loss of 137.9 μV / h.

In this search, a correlation between the fuel cell stack minimum output power (parameter **1** from the list in section 3.4.2) and minimum fuel consumption is observed. Only parameter sets with parameter a at around 7.9 kW perform well, in terms of fuel consumption. That correlation is used to reduce the computational work for all following optimisation runs, which are not allowed to alter that parameter anymore. The side objective of lowest possible fuel consumption is hereby directly addressed.

4.1.2 Minimum Fuel Cell Degradation Benchmark Case

With 8 parameters left to tweak, the optimisation run for the least fuel cell degradation case is carried out. The result is a representative voltage decay of 56.67 μV for one WLTC-3b driving cycle, or 113.3 μV / h. This case uses a fuel mass of 0.2773 kg of hydrogen, which equals 1.19 kg H_2 / 100 km.

As defined in section 2.3, the criterion for fuel cell stack's end-of-life is met, if the collective representative voltage decay exceeds 0.07 V. So the vehicle is able to be operated for 617.8 h in the WLTC-3b, before its fuel cell stack has reached its calculated end-of-life. That is considerably low, especially in comparison to the desired minimum lifetime of 6000 h, demanded for further success of FCHEVs.

Apart from that, a theoretical lifespan of only 1400.5 h would be reached if solely start-stop degradation would arise from the system's operation in the WLTC-3b. That shows that the implemented degradation model uses a selected pessimistic data-set to obtain a minimum FC stack lifetime. Therefore the expectable lifetime in reality should be higher.

4.1.3 Trade-off Behaviour between decreasing Fuel Consumption and reducing Fuel Cell Degradation

To examine the trade-off behaviour between the two benchmark cases, further optimisation runs are carried out. For each value of fuel cell degradation's weight w in the objective function (see Equation 3.4 for reference), an optimisation process is executed. Four different weightings are investigated, w = [0.25, 0.5, 0.75, 0.9], as the benchmarks already represent w = [0, 1]. The resulting non-dominated points, including the benchmark cases, are presented in Figure 4.1.

Assuming that optimal solutions between the two benchmark cases have been found, it can be concluded that the points in Figure 4.1 are part of the Pareto front of the associated multi objective optimisation problem.

On the one hand, the highest possible fuel cell degradation savings, for the given setup of EMS/vehicle model/degradation model, literally cost 3.55 % more fuel. On the other hand, the mitigable part of the overall fuel cell degradation benchmark is 28 % lower, in comparison with that of the fuel consumption benchmark case. An example case, which uses approximately half of the savings for each individual objective, is chosen and marked in the Pareto front in Figure 4.1. It is used for demonstration purposes in the following sections and images.

Figure 4.2 takes a closer look on the fuel cell degradation's origin, showing the two benchmark cases at the sides, and the example trade-off-case in the middle. It reveals, that the model assesses the galvanostatic degradation ranges between 6 to7 % of the total amount of degradation, throughout the three shown cases. The degradation optimisation

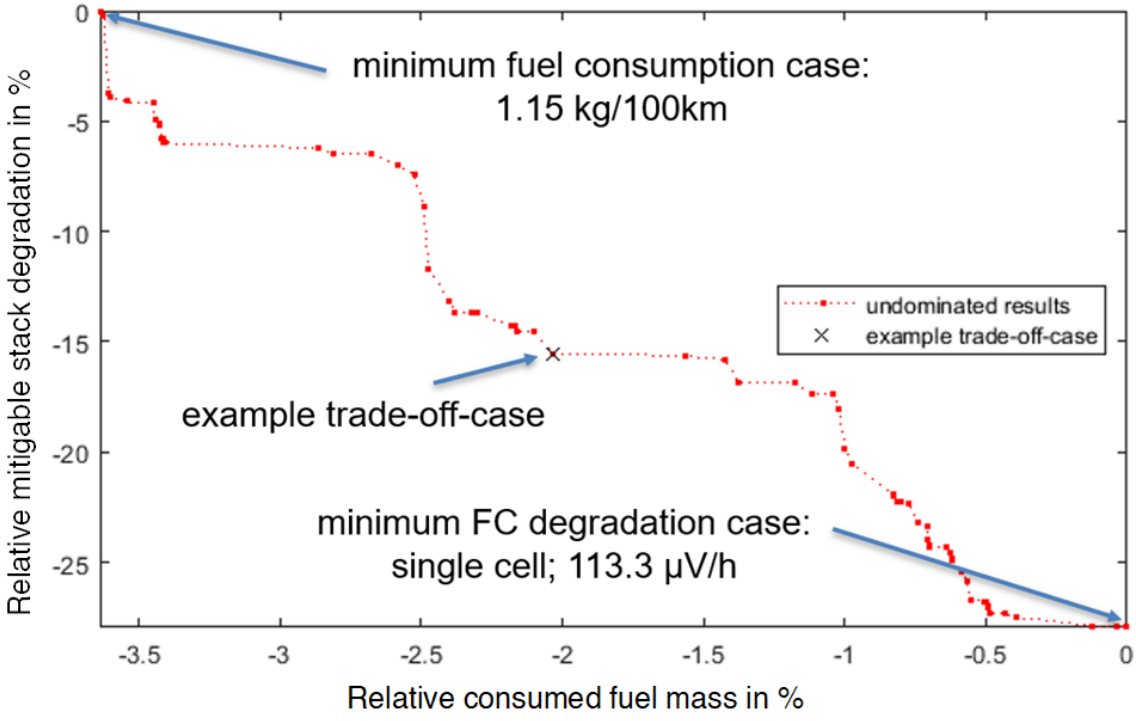

Figure 4.1: Trade-off behaviour between minimum fuel consumption and minimum fuel cell degradation, depicted by all other found non-dominated cases.

leads to an increased relative amount of galvanostatic degradation, although its absolute value is reduced from 8.36 μV / h to 7.92 μV / h.

The comparison in Figure 4.2 shows the effectiveness of the degradation optimisation, as a decrease of the relative amount of load cycling fuel cell degradation is perceptible. Absolute numbers back that visible trend up, the model calculated representative voltage loss is decreased from 79.5 μV / h in the fuel consumption benchmark case to 55.4 μV / h in the degradation benchmark case by the conducted parameter optimisation.

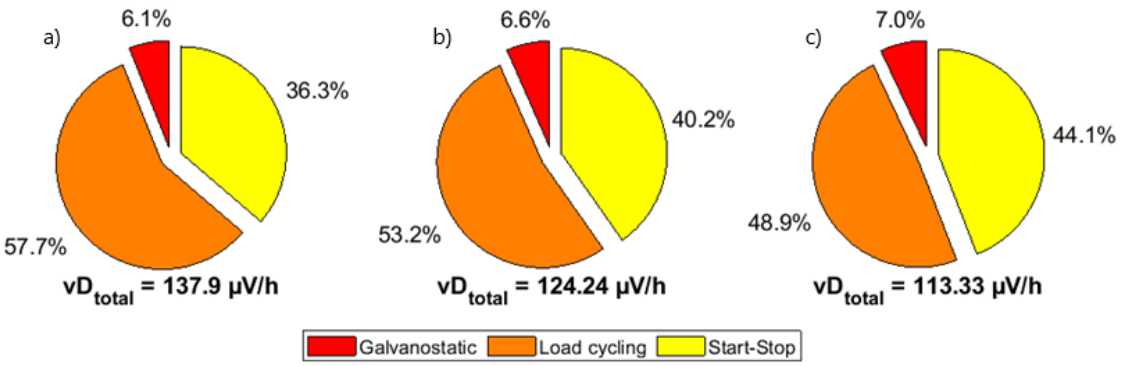

Figure 4.2: Resulting representative degradation for three cases: a) fuel consumption benchmark case; b) example trade-off-case; c) fuel cell degradation benchmark case

The amount of start-stop degradation during the driving cycle cannot be influenced in this investigation, as the developed EMS is an always-on strategy. That induces a constant additional amount of assumed degradation to the galvanostatic and load cycling voltage decay, once per driving cycle for all investigated cases. In the three exemplary cases in Figure 4.2, it is responsible for an amount of between 36.3 % and 44.1 % of the overall assessed degradation.

4.2 Interpretation of the Results

The retrieved results are examined and discussed in the following section, also precaution is given and limitations are highlighted. All the vehicle's sub-models and its EMS proof to work correctly throughout the investigations.

4.2.1 General Performance of the Three Example Cases

Brief information on the overall performance of the three example cases is given here. The two most important boarder conditions are met in each case. On the one hand, the driving task is correctly absolved, and on the other hand the HV-battery is operated charge sustaining. Hence the results might be legitimately compared against those of other vehicles/researches in the WLTC-3b.

Figure 4.3 underpins the charge sustaining operation of each case, although they produce different time profiles of the battery's SoC. It is further revealed, that all three cases recharge the HV-battery one time per driving cycle. The minimum fuel consumption case (red) and the example trade-off-case (orange) begin to charge the battery after roughly 300 s of driving, while the minimum degradation case (yellow) enters the recharge mode approximately 500 s after the start. The charging mode is easily identified from the graphs, as the SoC is almost linearly increasing by that time.

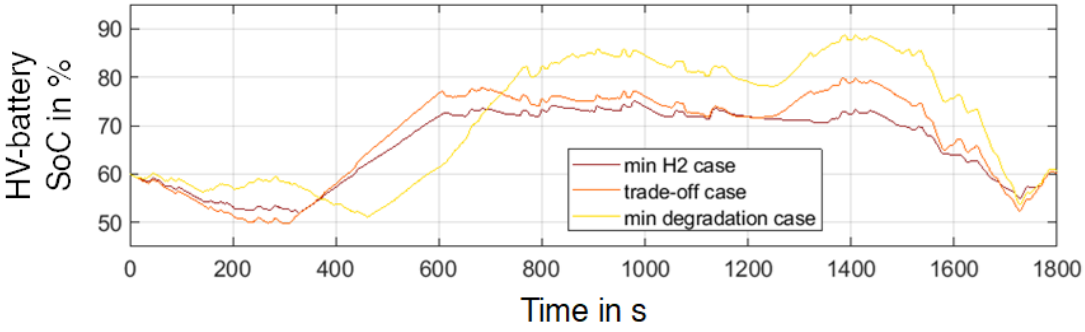

Figure 4.3: Time course of the HV-battery's SoC, for the three example cases.

Apparently, the minimum fuel cell degradation case allows even more use of the HV-battery's capacity, compared to the example trade-off-case and the fuel consumption benchmark case. That becomes clear from Figure 4.3 as well, because in the degradation benchmark case more energy is charged into the battery.

As a side note, all individual cases use the battery over a much wider SoC interval, than that observed in the real vehicle. Only around 3 % of SoC variation are measured in the real vehicle, compared to 20 % to 35 % in this work [16, 18].

4.2.2 Fuel Consumption Analysis

The fuel consumption of the corresponding benchmark case is 0.2674 kg for one WLTC-3b, which equals to 1.15 kg / 100 km. To qualitatively point out the simulated vehicle's performance in terms of fuel efficiency, a comparison to measurements [16, 22] of the Toyota Mirai Gen. 1 is done. Table 4.1 summarises the fuel consumption benchmark simulation results, together with the measurement results of the vehicle in the WLTC-3b.

Table 4.1: WLTC-3b results comparison.

Data set	Simulation	Measurement [16]
Consumed $W_{Eelectrical\ Machine}$ in MJ	13.3915 [5]	
Consumed W_{H_2} in MJ	32.08 [6]	22.824 [6]
Consumed m_{H_2} in kg	0.26742	0.190263 [6]
$\eta_{Fuel\ Cell\ System,\ avg}$ in 1	0.4174	0.569
theoretical minimum $m_{H_2,\ min}$ in kg	0.19619	0.17525
$\eta_{Fuel\ Cell\ System,\ max}$ in 1	0.569	0.637

As the electrical machine's work $W_{Electrical\ Machine}$ is not provided in [16], the simulation result is carried over in Table 4.1. This introduces only minor inaccuracy, according to the previously carried out validation of the electromechanical vehicle model. A substantial difference between the measured and the simulated vehicle is their respective FCS, as the model uses measurement data from a standalone system on the IFA TU Wien FC test stand. See section 3.1 and 3.2.1 for details, as well as Figure 4.6.

The consumed hydrogen mass for one driving cycle, m_{H_2} in Table 4.1, is a direct result of the simulation environment, while in [16] the hydrogen-based energy W_{H_2} is stated. Both results are conversed with hydrogen's Lower Heat Value of 119.96 MJ / kg, to obtain

[5] Result from Simulation.
[6] Calculated with Lower Heat Value of 119.96 MJ / kg, according to [16].

comparability. Each FCS's measured maximum efficiency $\eta_{Fuel\ Cell\ System,\ max}$ is stated and they are used for further categorisation of the simulation results. The given data of $\eta_{Fuel\ Cell\ System,\ max}$ in Table 4.1 reveals, that the Mirai's FCS has a 12 % higher peak efficiency than that of the simulation model.

If each respective FCS would be able to produce the work W_{EM} at its peak efficiency, the theoretically demanded hydrogen mass $m_{H_2,\ min}$ from Table 4.1 would be consumed. The Mirai FCS needs approximately 8.6 % more hydrogen than the theoretically possible minimum of 0.17525 kg.

Whereas the simulation model's FCS uses 36.3 % more fuel mass, than its respective hypothetical minimum. That makes up for an average FCS efficiency of 41.7 % for the simulation, and 56.9 % for the real vehicle.

Besides the obviously lower peak efficiency of the model implemented FCS, also the power at which the maximum system efficiency occurs is different. Figure 4.4 shows measurement results of the real vehicle's FCS. The Mirai system's peak efficiency occurs in the region of 7 kW, whereas the model reaches the maximum efficiency at roughly 25 kW.

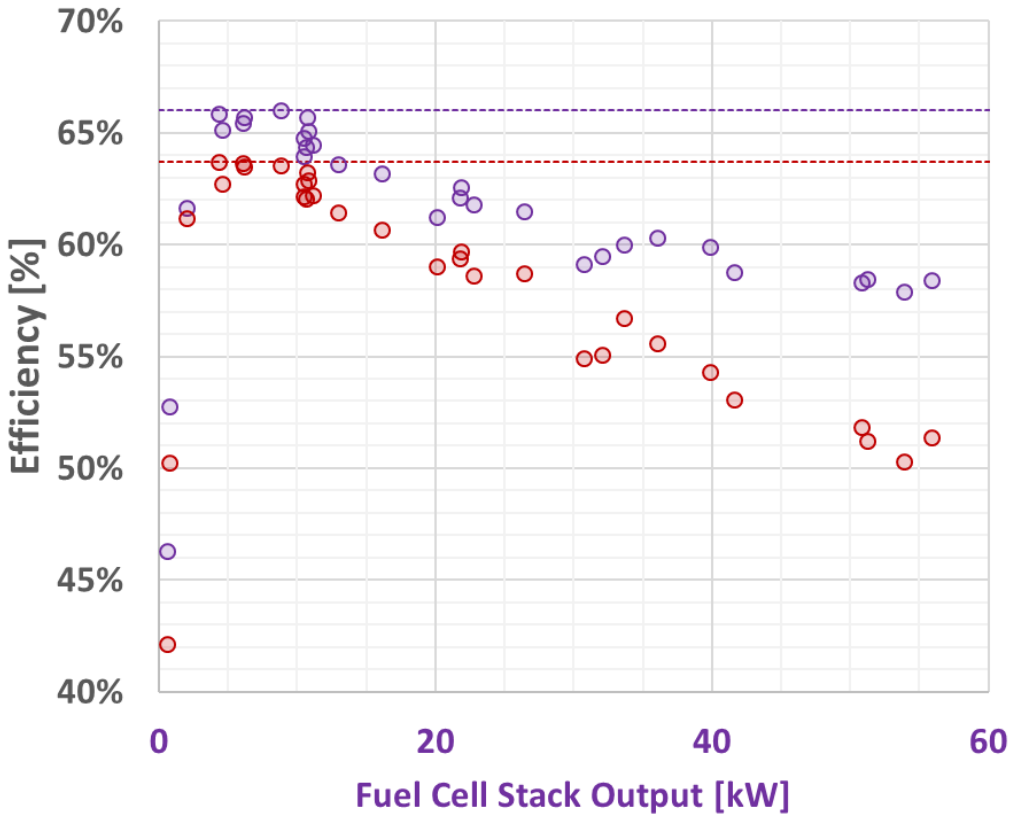

Figure 4.4: Toyota Mirai FC stack and FCS efficiency. Purple: Stack efficiency; Red: System efficiency [16].

Figure 4.5 shows the simulation result of the EM power demand, together with the power level of the Mirai's and the model's FCS maximum efficiency. It could be argued, that the chosen model FC stack in this work is overpowered for the given application, as the EM hardly loads the FCS enough to maintain efficient operation. A FCS's efficiency sinks rapidly, at power levels below its maximum efficiency, as seen in Figure 4.4 and 3.9. That is one of the reasons for the observed high level of fuel consumption of the simulation.

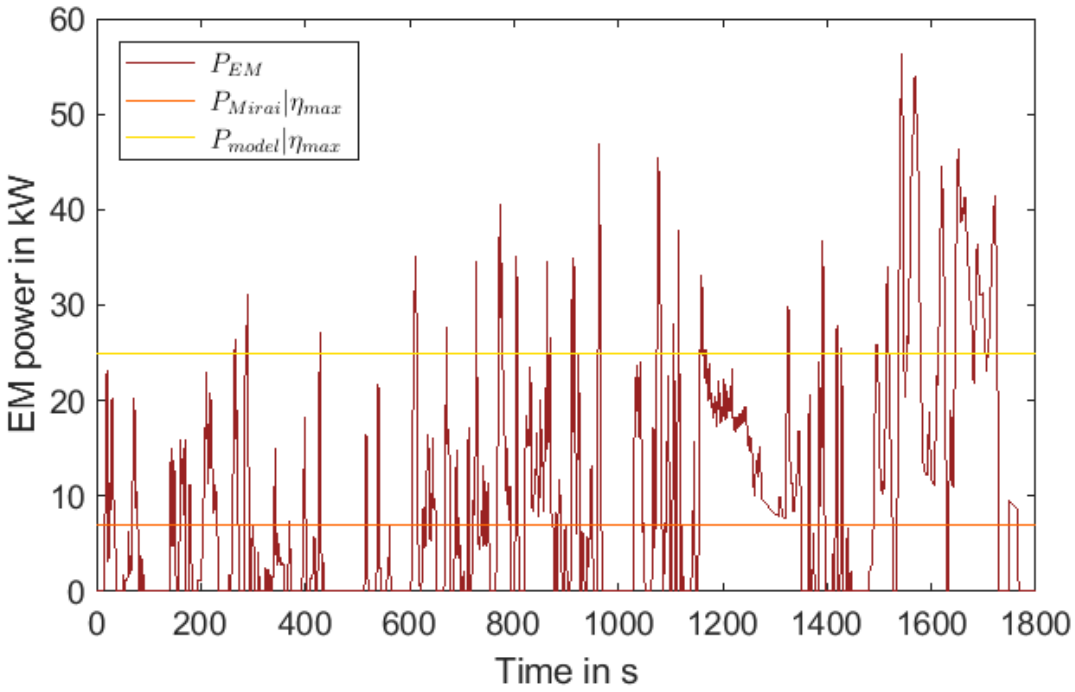

Figure 4.5: Simulaiton EM power demand in the WLTC-3b, and power level of Mirai and model $\eta_{FCS,max}$ occuring.

One more systematic reason for the lower fuel efficiency of the simulated vehicle despite its "size", is the comparably high power demand of its BoP components. Figure 4.6 is derived from detailed BoP components measurements [22], gathered in the ADAC ECO Test cycle. It shows the summed power demand of the hydrogen recirculation pump and the coolant pump, and separately the air compressor's demand. It can be seen, that especially in low load regions, the model ancillaries are outperformed by the Mirai's components.

Figure 4.6 shows, that the model's H_2 and coolant pumps use roughly three times the power of the respective Mirai's pumps, throughout the whole operation range. Contrary is the trend for both system's air compressors. They use similar amounts of power in low load regions, with a higher power consumption for the Mirai compressor at middle to high FC stack load regions.

The optimisation process for minimum FC degradation alters the system's operation, so an increased fuel demand is expected for deviations from that minimum. Figure 4.1 shows

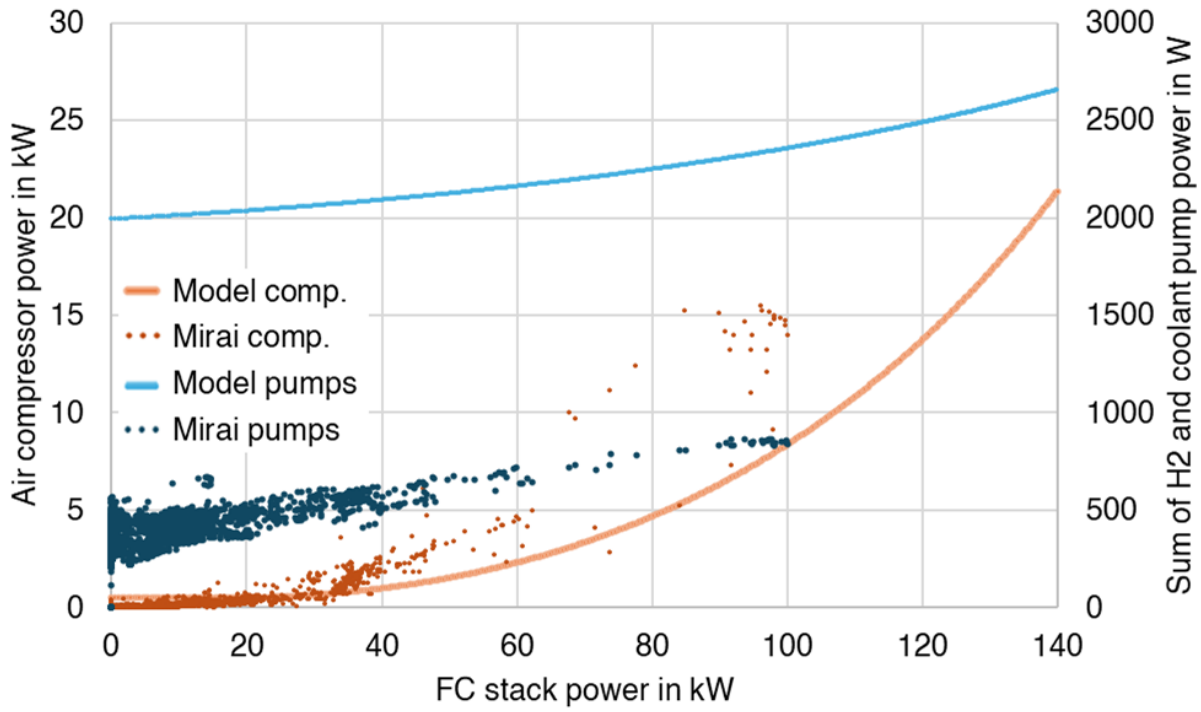

Figure 4.6: Model data vs. measurement [22] in the ADAC ECO Test cycle.

the results of feasible variants of parameter sets, which are characterised by a decreased fuel cell degradation, compared to the fuel consumption benchmark case.

As stated in section 3.4.2, the EMS's parameters are about to load shift the FCS and therefore enable efficient power generation. Although the degradation optimised cases tendentially operate the FCS more likely at its peak efficiency, only small relative savings of about 3.5 % between minimised fuel consumption and minimised FC degradation strategy are possible. The fuel cell degradation benchmark case achieves a fuel consumption of 0.2773 kg of hydrogen, which equals 1.19 kg H_2 / 100 km.

The next section's Figure 4.7 shows clearly the applied load shifting for the degradation optimised cases. It is also observed, that the EMS operates the stack a great amount of time slightly below the system's maximum efficiency point. That is another hint for an overpowered FC stack.

In comparison with the fuel consumption optimised cases, another reason for the increased fuel consumption of the per se more efficient FCS operation of the degradation optimised cases is the vehicle's efficiency chain. In times, where the applied phlegmatsation or load shift causes the stack to produce more power than actually required, the energy is stored in the HV-battery. At other times, the EMS discharges the battery to shift the load point of the FC stack to a lower level. This way the energy has to pass the HV-battery's DC/DC converter twice, and the battery's charging and discharging efficiency are applied before the energy can be used for vehicle propulsion.

4.2.3 Galvanostatic Degradation Analysis

To gain deeper understanding of how the conducted fuel cell degradation mitigation works, the output power spectrum of the fuel cell stack is investigated. Figure 4.7 shows the time the stack spends at a certain load point during a simulation run of the driving cycle.

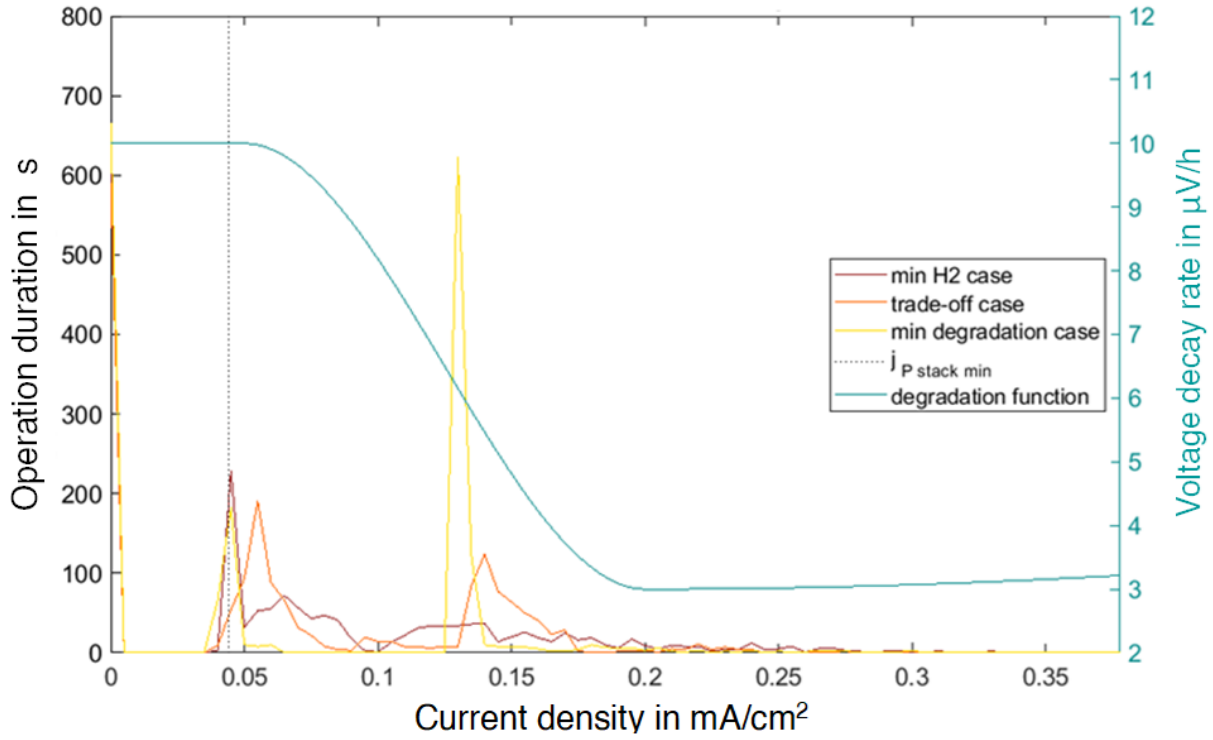

Figure 4.7: Analysis of stack operation time at various load levels, together with corresponding galvanostatic voltage decay model function.

Only a part of the potentially allowed fuel cell stack current density is shown in Figure 4.7, to emphasise the most notably areas of the diagram. For better orientation, the degradation model function and a vertical line at the current density, corresponding to the minimum stack power $j\,|_{P\ stack,\ min}$, are plotted in the same diagram.

The minimum consumption benchmark case runs the stack over a wide spread region of loads, with considerably more time spent in idle and at $j\,|_{P\ stack,\ min}$. This is caused by the always-on strategy, combined with no permitted operation between idle and the minimum stack output power threshold. That changes for the trade-off-case, where an increased operation duration in the region of the maximum fuel cell system efficiency, see Figure 3.9 for reference, is observed. The most extreme stack output power spectrum is produced by the degradation mitigation benchmark case. Here the fuel cell system is mainly operated close at its peak fuel efficy load point.

4.2.4 Load-Cycling Degradation Analysis

The major contribution to the fuel cell degradation is made by the load-cycling category, it accounts for about half of the overall degradation. The top part of the double-graph in Figure 4.8 shows the stack output power over the driving cycle time. Below that, the cumulative load-cycling voltage decay for the same three representative cases is shown. From a visual inspection can be derived, that the fuel efficiency benchmark case drifts faster off the other cases, in more dynamic driving profile regions.

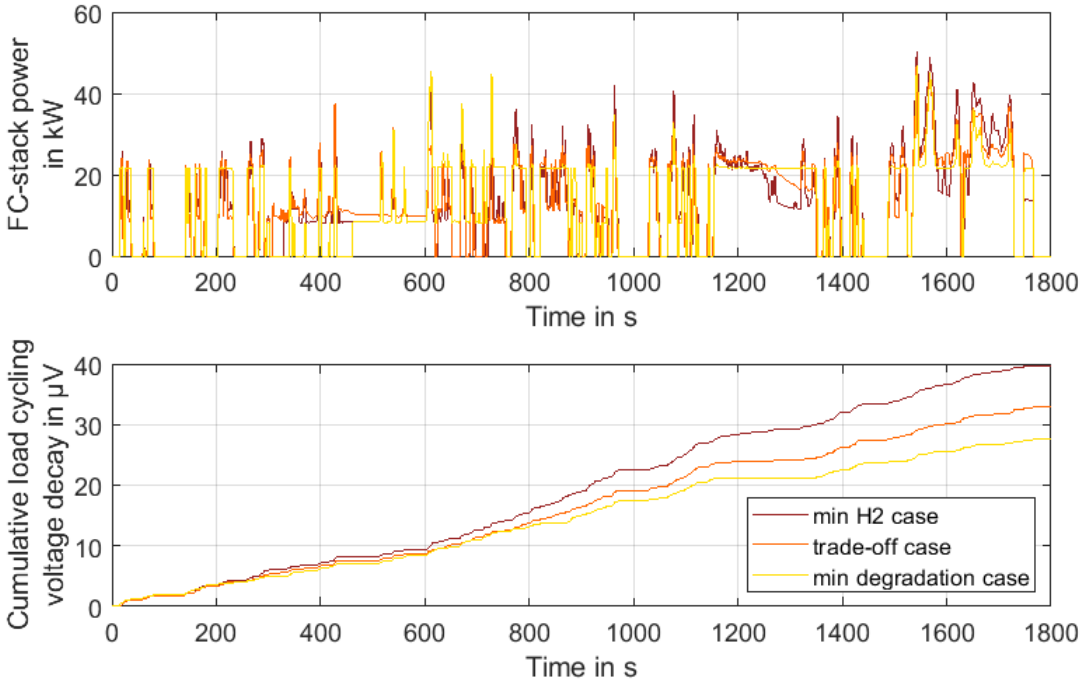

Figure 4.8: Results of the three cases. Top: Fuel cell stack output power. Bottom: Cumulated load-cycling voltage decay.

A close look at the timespan of 1100 s to 1800 s of driving cycle time can be taken in the graphs of Figure 4.9. The bottom graph takes on a different approach to show the effectiveness of the conducted load-cycling degradation mitigation. It shows the difference between the fuel consumption benchmark case and the degradation benchmark case in dark green, and the difference between the example trade-off-case and the degradation benchmark case in turquoise. That graph emphasises the trend, which is already observable in Figure 4.8.

The top section of Figure 4.9 shows enlarged the fuel cell stack's power output for the three cases. In comparison to the fuel efficiency benchmark case, in certain power demand regions the trade-off-case and the degradation benchmark case apply a more steady power demand on the stack. I.e. the region between 1150 s and 1350 s visualise intended phlegmatisation, applied by the EMS. However, the developed phlegmatisation

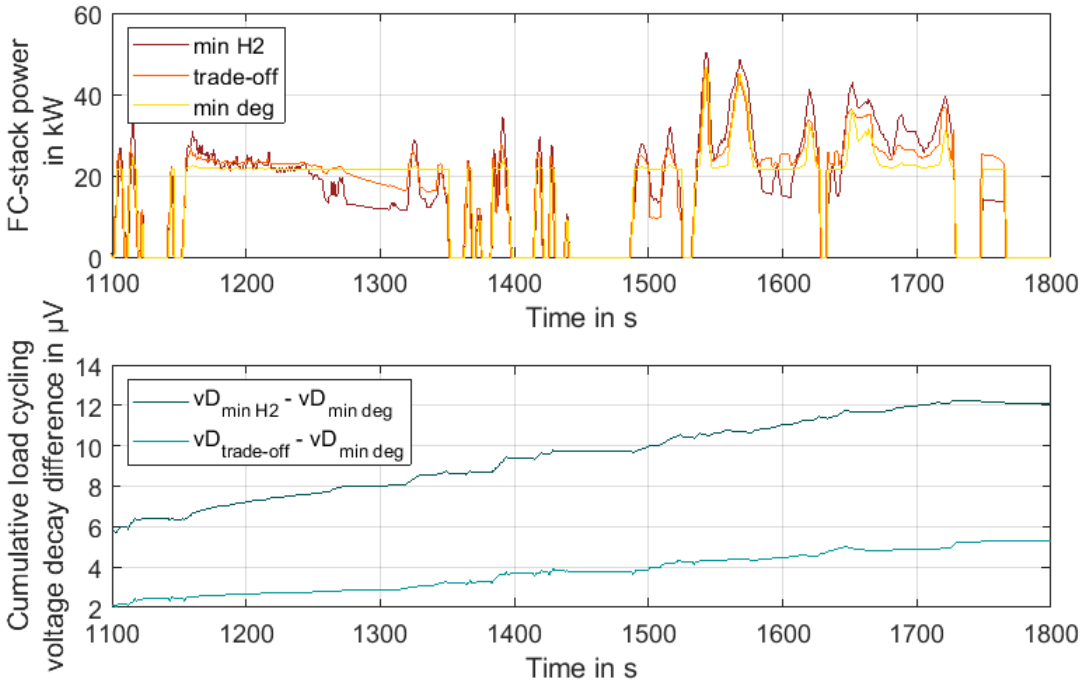

Figure 4.9: Top: Zoomed timeline of the fuel cell stack power output for the three cases. Bottom: Difference of cumulative voltage decay between the cases in that timeframe.

strategy is less effectively reducing the load fluctuations between 1530 s and 1730 s. The main reasons therefore are the HV-battery maximum power output limitation, the algorithm's choice of the "position" (parameter P_2) and "width" (parameters P_3 and P_4) of the phlegmatisation band, and the algorithm's choice for the battery's discharge power factor (parameter P_9). Further notes about the EMS's limitations are found below in section 4.2.5.

4.2.5 Limitations of the used Approach

The optimisation for degradation mitigation alters the EMS parameters to conduct phlegmatisation within given ranges of stack power demand. To still meet the driver's power demand, load steps are applied to the fuel cell system at the outer boarders of the phlegmatised domains. Common engineering sense would suggest to avoid exactly that behaviour, as the whole FCS has to react to the stepwise change in power output. The effect is elaborated in more detail Figure 4.10, where again the three exemplary cases are compared. In this histogram, the number of events of load changes at the corresponding power change rate is plotted for a single cell. This negative side effect is introduced by the structure of the hybridisation function and the chosen degradation modelling approach of the fuel cell degradation model.

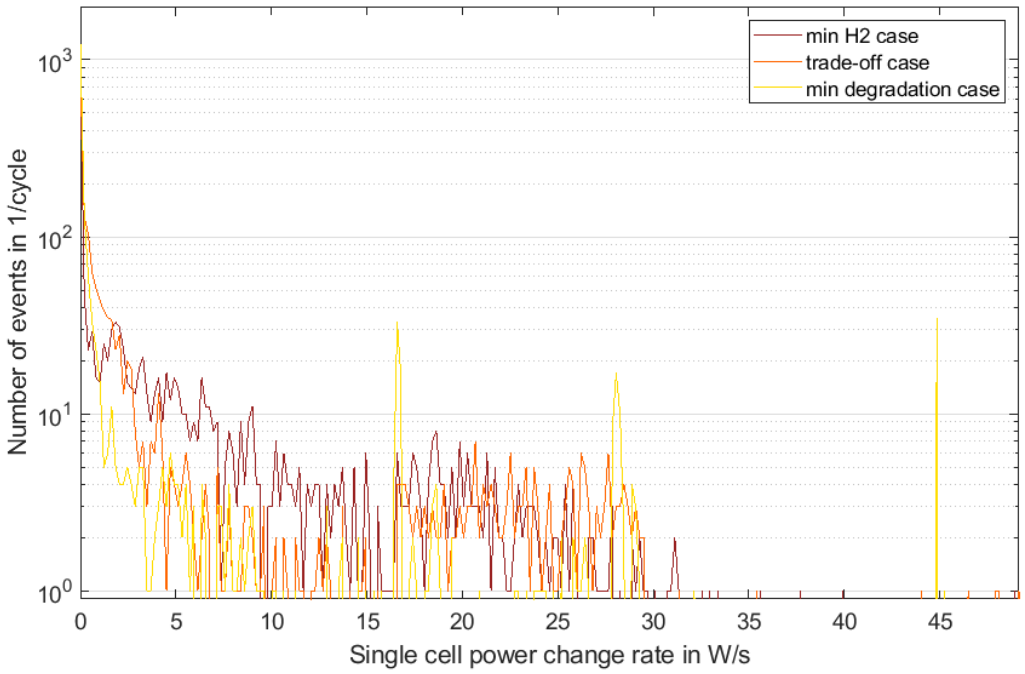

Figure 4.10: Analysis of the number and gradients of applied load changes for the fuel consumption benchmark case, the trade-off-case, and the degradation benchmark case.

The minimum fuel consumption benchmark case causes a comparably large overall number of load changes, but their majority is applied at rates of 30 W / s and below. The example trade-off-case performs different, as a slight shift towards higher power change rates around 28 W / s can be observed. However it reduces applied load changes between 16 W / s and 4 W / s, compared to the fuel consumption benchmark case. The degradation benchmark case reduces the number of applied load changes throughout the range, without a few exceptions. Noteworthy is the heavily increased number of events at 45 W / s. The optimisation of the phlegmatisation function therefore seems to focus on the reduction of necessary load change events, without adequately addressing the height of the occurring load steps.

However, it should be noted that large load step heights promote mechanical and thermal stress in combination with inhomogeneity to the species concentration and water distribution inside the fuel cell stack, therefore its degradation is fostered [3, 45, 50].

4.2.6 Degradation Results in Context of Research Literature

Figure 4.11 shows the results of degradation categorisation of other researches. These results are derived from other test cycles than the WLTC-3b, so this comparison has to be made with that in mind. Compared to the results of the here presented degradation

model (see Figure 4.2 for reference), [29] observes similar shares of each category on the total degradation amount, Figure 4.11 a).

Qualitatively different are the results of [5]. The absolute value of start-stop degradation is there given at 24 μV per cycle, which is almost the same as in this work (25 μV per cycle). The degradation due to load-cycling is stated to be similar to that of galvanostatic degradation, see Figure 4.11 b). This is in contrast to the here elaborated results. The main reason therefore is, that in [5] a load-cycling degradation rate of 0.0441 $\mu V/(\Delta kW/cell)$ is used, which is approximately 200 times smaller than the mean value used in this work's model. No detail is given on stack data besides a 24 V nominal voltage and 4.8 kW output power, which hinders closer cross comparison. However, it is stated, that the used degradation rate is derived from the fuel cell manufacturer data sheet. Compared with other researches, that is 7 to 70 orders of magnitude smaller than the degradation rate used there [3]. Another cause for the low cumulated load cycling degradation might be the considerably larger capacity traction battery of the vehicle in [5], relatively spoken. The 4.8 kW stack is used in combination with a 2 kWh battery, while here the stack has 140.5 kW and only 1.6 kWh of battery energy capacity.

This ratio, together with the presented results in [5], hints towards more of a range-extender like operation of the fuel cell, which is substantially different to the highly volatile stack loading of this work's application and that of [29].

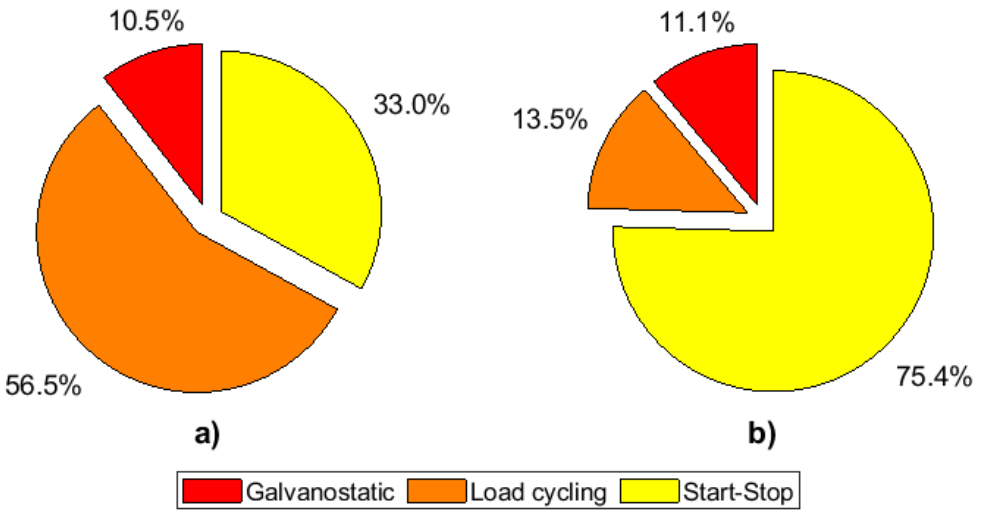

Figure 4.11: Degradation categorisation of other researches: a) Gathered on an accelerated stress test [29]; b) Gathered from a fuel consumption optimised run of a recorded real driving cycle [5].

5 Conclusion

A longitudinal vehicle dynamics simulation model of a FCHEV is set up. The first generation Toyota Mirai serves as reference for the model's electromechanical part. Measurements of a real vehicle performing the ADAC ECO Test cycle at the IFA/TU Wien chassis dynamometer are used to validate that model part. An equivalent circuit model for the fuel cell stack and lookup-tables for the balance of plant components are parametrised with measurement data from the IFA/TU Wien fuel cell system test stand.

A literature review is conducted, to develop a data-driven fuel cell degradation model. Based on the stack power output, the model calculates a galvanostatic, and a load-cycling degradation term. Every startup&shutdown cycle of the fuel cell system evokes a constant amount of additional degradation to the model calculated value. The output of the model is a single cell's voltage loss, compared to a new cell at a representative current density.

The focus of the developed powertrain's EMS lies in features, dedicated to fuel efficient operation, and to the alleviation of the fuel cell degradation progress. That is mainly achieved via fuel cell stack load point shifting and phlegmatisation, which exploits the overlapping area of operational ranges with high fuel economy and low degradation progress.

Numerical investigations are conducted in the WLTC-3b driving cycle via numerical optimisation of the vehicle model's EMS parameter values. The search for a benchmark case with the minimum possible fuel consumption of the given simulation setup results in 1.15 kg H_2 / 100 km. Compared to a measurement of a real vehicle at 0.818 kg H_2 / 100 km, the simulation results point towards a generally low fuel efficiency performance. Reasons therefore are a lower peak efficiency of the implemented FCS, paired with an overly high power output capability for the given application.

A second benchmark is searched for, in terms of minimum possible fuel cell degradation. Compared to the minimum fuel consumption benchmark case, it uses 3.55 % more fuel, but avoids 28 % of mitigable fuel cell degradation. Together with the non mitigable start-stop cell performance derating, the degradation benchmark reaches an overall rate of 113.3 μV / h during vehicle operation. The degradation benchmark case predicts an expectable fuel cell lifetime of 617.8 h, which is considerably low in comparison with the long-term development target of 6000 h. That has to be seen in context of a theoretical lifespan of 1400.5 h, which would be reached if only start-stop degradation would arise from the system's operation in the WLTC-3b. That underlines, that the degradation model input data is chosen pessimistic, but nevertheless a useful tool to assess and mitigate fuel cell degradation is presented in this work.

A weighted sum method is developed, to merge the two conflicting results of fuel cell degradation and fuel efficiency in one single objective function, so that the problem can be handled by the optimisation algorithm. It enables the user to direct the optimisation algorithm into the solution area of most interest and therefore is a crucial part for an effective search of the Pareto front between the two benchmark cases. Thereby the trade-off behaviour of the two contrary objectives is highlighted. An example trade-off-case is chosen, which achieves approximately half of the possible maximum savings of each individual objective. Compared with the fuel efficiency benchmark case, the example trade-off-case yields a 15 % lower mitigable degradation rate, while it uses 2 % more fuel. This case demonstrates the effectiveness of the optimisation procedure.

To the best knowledge of the author, there is generally not much data available to build a degradation model like this. There is no directly correlated measurement data available in literature, so there is no way to precisely model the impact of the rate of load variations. The incorporated model therefore does not ratify load change rates, even though this would enable a more differentiated assessment of the fuel cell's load profile.

The procedures of accelerated stress tests for fuel cells, which provide the parametrisation data for the degradation model, are subject to research themselves. Future research findings of degradation investigations can be used to re-parametrise and even extend the presented model and therefore open up more insights to the trade-off behaviour between fuel cell degradation and fuel consumption.

Bibliography

[1] U.S. Department of Energy, Fuel Cell Technologies Office: Multi-Year Research, Development and Demonstration Plan, Planned program activities for 2011-2020, https://www.google.com/url?sa=t&source=web&rct=j&opi=89978449&url=https://www.energy.gov/sites/prod/files/2014/12/f19/fcto_myrdd_full_document.pdf&ved=2ahUKEwjr9qGej_aFAxWsVPEDHWWODTwQFnoECBcQAQ&usg=AOvVaw1JgsYf2PcUTUcTASjeGlb-, 2012.

[2] Dicks, A.L.; Rand, D.A.J.: Fuel Cell Systems Explained, Wiley, ISBN: 978-1-118-70697-8, 2018.

[3] Lorenzo, C.; Bouquain, D.; Hibon, S.; Hissel, D.: Synthesis of degradation mechanisms and of their impacts on degradation rates on proton-exchange membrane fuel cells and lithium-ion nickel–manganese–cobalt batteries in hybrid transport applications, Reliability Engineering and System Safety, 212 (2021), 107369.

[4] European Union: HORIZON 2020; Material, Operating Strategy and Reliability Optimisation for Lifetime Improvements in heavy Duty Trucks, [Online] https://cordis.europa.eu/programme/id/H2020_FCH-01-2-2020/en. Information accessed on 16.2.2023, 2020.

[5] Fletcher, T.; Thring, R.; Watkinson, M.: An Energy Management Strategy to concurrently optimise fuel consumption & PEM fuel cell lifetime in a hybrid vehicle, International Journal of Hydrogen Energy, 41 (2016), 21503-21515.

[6] Hofmann, P.: Hybridfahrzeuge, Springer, ISBN: 978-3-662-66893-1, 2023.

[7] Elgowainy, A.: Electric, Hybrid, and Fuel Cell Vehicles, Springer, ISBN: 978-1-0716-1492-1, 2021.

[8] HONDA: Honda Clarity Fuel Cell 2017 - Pressemappe, Manufacturer press Information, https://hondanews.eu/at/de/download/107266/pdf/pdf, 2017.

[9] American Honda Motor Co., I.: Website: https://hondanews.com, [Online] https://hondanews.com/en-US/honda-automobiles/releases/release-fdf2b7a7fd6542489b0d45ede2248a55-2017-honda-clarity-fuel-cell-specifications/. Information accessed on 22.4.2024.

[10] Hyundai Motor Deutschland GmbH: Hyundai ix35 Fuel Cell, Technische Daten, Manufacturer datasheet, https://www.hyundai.news/newsroom/dam/de/Pressemappen/ix35_Fuel_Cell/2018/ix35_Fuel_Cell_2018_3_Technische_Daten.pdf, 2018.

[11] Geringer, B.; Tober, W.; Höflinger, J.: Studie zur messtechnischen Analyse von Brennstoffzellenfahrzeugen | Hyundai ix35 FCEV (No. B16034), Research Report, 2016.

[12] Hyundai Motor Deutschland GmbH: Hyundai Nexo, Preise und technische Daten, Manufacturer datasheet, https://www.hyundai.news/newsroom/dam/de/Pressemappen/Nexo/hyundai-nexo-sep2018-technische-daten.pdf, 2018.

[13] Sery, J.; Leduc, P.: Fuel cell behavior and energy balance on board a Hyundai Nexo, International Journal of Engine Research, 23 (2021), 709-720.

[14] Mohrdieck C.: Wasserstoff und Brennstoffzellen. Vorlesungsunterlagen TU Wien, 2019.

[15] Mohrdieck, C.; Dehn, S.: Intelligentes Brennstoffzellen-Plug-in-Hybrid-Antriebssystem, ATZ, 122. Jahrgang (01/2020) pp. 64–73.

[16] Lohse-Busch, H.; Duoba, M.; Stutenberg, K.; Iliev, S.; Kern, M.; Richards, B.; Christenson, M.; Loiselle-Lapointe, A.: Technology Assessment of a Fuel Cell Vehicle: 2017 Toyota Mirai, Argonne National Laboratory, Report # ANL/ESD-18/12, 2018.

[17] Toyota Deutschland GmbH: Mirai Preise und Fakten, Manufacturer datasheet, https://www.toyota.de/content/dam/toyota/nmsc/germany/downloads/mirai/Toyota_PL_Mirai_06_22_b_final.pdf, 2022.

[18] Pielecha, I.; Szałek, A.; Tchorek, G.: Two Generations of Hydrogen Powertrain - An Analysis of the Operational Indicators in Real Driving Conditions (RDC), Energies, 15 (2022), 13.

[19] American Honda Motor Co., I.: Website: https://www.greencarcongress.com, [Online] https://www.greencarcongress.com/2015/10/20151027-clarity.html. Information accessed on 22.4.2024.

[20] Pielecha, I.: Modeling of Fuel Cells Characteristics in Relation to Real Driving Conditions of FCHEV Vehicles, Energies, 15(18) (2022) p. 6753.

[21] Blue Energy Co., Ltd.: Blue Energy's Lithium-ion Batteries to be used in Honda's CLARITY FUEL CELL, News Release, https://www.gs-yuasa.com/webdata/img/gs160409074527/pdf_gs_160709311419.pdf, 2016.

[22] Geringer, B.; Tober, W.: Studie zur messtechnischen Analyse von Brennstoffzellenfahrzeugen | Toyota Mirai, Österreichischer Verein für Kraftfahrzeugtechnik, 2019.

[23] Pan, J.; Yang, J.; Yan, D.; Pu, J.; Chi, B.; Li, J.: Effect of thermal cycling on durability of a solid oxide fuel cell stack with external manifold structure, International Journal of Hydrogen Energy, 45 (2020), 17927-17934.

[24] Hofmann, P.; Höflinger, J.: Brennstoffzellenantriebe. Vorlesungsunterlagen TU Wien, 2019.

[25] Yumiya, H.; Kizaki, M.; Asai, H.: Toyota Fuel Cell System (TFCS), World Electric Vehicle Journal, 7 (2015), WEVJ7-0085.

[26] TOYOTA MOTOR CORPORATION: TOYOTA Technical Review Vol. 66, ISSN: 0916-7501, 2021.

[27] Galović, J.: Literaturrecherche: Feuchtigkeitsmanagement von PEM-Brennstoffzellenantrieben im Automotive-Bereich, Projektarbeit am IFA der TU Wien 2017 02 14, 2017.

[28] Wang, G.; Huang, F.; Yu, Y.; Wen, S.; Tu, Z.: Degradation behavior of a proton exchange membrane fuel cell stack under dynamic cycles between idling and rated condition, International Journal of Hydrogen Energy, 43 (2018), 4471-4481.

[29] Pei, P.; Chang, Q.; Tang, T.: A quick evaluating method for automotive fuel cell lifetime, International Journal of Hydrogen Energy, 33 (2008), 3829-3836.

[30] Pahon, E.; Jemei, S.; Steiner, N.Y.; Hissel, D.: Effect of Load Cycling on the Performance of Fuel Cell Stacks, IEEE Vehicle Power and Propulsion Conference (VPPC), (2019) pp. 1–4.

[31] Chen, H.; Pei, P.; Song, M.: Lifetime prediction and the economic lifetime of Proton Exchange Membrane fuel cells, Applied Energy, 142 (2015), 154-163.

[32] Chu, T.; Zhang, R.; Wang, Y.; Ou, M.; Xie, M.; Shao, H.; Yang, D.; Li, B.; Ming, P.; Zhang, C.: Performance degradation and process engineering of the 10 kW proton exchange membrane fuel cell stack, Energy, 219 (2021), 119623.

[33] Collier, A.; Wang, H.; ZiYuan, X.; Zhang, J.; Wilkinson, D.P.: Degradation of polymer electrolyte membranes, International Journal of Hydrogen Energy, 31 (2006), 1838-1854.

[34] Stolten, D.: Hydrogen and Fuel Cells, Wiley-VCH, ISBN: 978-3-527-32711-9, 2010.

[35] Yang, Z.; Ball, S.; Condit, D.; Gummalla, M.: Systematic Study on the Impact of Pt Particle Size and Operating Conditions on PEMFC Cathode Catalyst Durability, Journal of The Electrochemical Society, 158 (2011), B1439-B1445.

[36] Jahnke, T.; Baricci, A.; Rabissi, C.; Casalegno, A.: Physical Modeling of Catalyst Degradation in Low Temperature Fuel Cells: Platinum Oxidation, Dissolution, Particle Growth and Platinum Band Formation, Journal of The Electrochemical Society, 167 (2020), 013523.

[37] Bae, S.J.; Kim, S.J.; Lee, J.H.; Song, I.; Kim, N.I.; Seo, Y.; Kim, K.B.; Lee, N.; Park, J.Y.: Degradation pattern prediction of a polymer electrolyte membrane fuel cell stack with series reliability structure via durability data of single cells, Applied Energy, 131 (2014), 48-55.

[38] Görke, D.: Untersuchungen zur kraftstoffoptimalen Betriebsweise von Parallelhybridfahrzeugen und darauf basierende Auslegung regelbasierter Betriebsstrategien, Springer, ISBN: 978-3-658-14162-2, 2016.

[39] Paganelli, G.; Ercole, G.; Brahma, A.; Guezennec, Y.; Rizzoni, G.: General supervisory control policy for the energy optimization of charge-sustaining hybrid electric vehicles, JSAE Review, 22 (2001), 511-518.

[40] Tran, D.D.; Vafaeipour, M.; El Baghdadi, M.; Barrero, R.; Van Mierlo, J.; Hegazy, O.: Thorough state-of-the-art analysis of electric and hybrid vehicle powertrains: Topologies and integrated energy management strategies, Renewable and Sustainable Energy Reviews, 119 (2020) p. 109596, ISSN:1364-0321.

[41] Steindl, C.; Hofmann, P.: Systematic Development Approach for a Hybrid Electric Powertrain Using Fuel-Cell-in-the-Loop Test Methodology, SAE Technical Paper 2023-01-0494.

[42] Markel, T.; Brooker, A.; Hendricks, T.; Johnson, V.; Kelly, K.; Kramer, B.; O'Keefe, M.; Sprik, S.; Wipke, K.: ADVISOR: a systems analysis tool for advanced vehicle modelling., Journal of power sources, 110 (2002), 255-266.

[43] Mayur, M.; Gerard, M.; Schott, P.; Bessler, W.G.: Lifetime Prediction of a Polymer Electrolyte Membrane Fuel Cell under Automotive Load Cycling Using a Physically-Based Catalyst Degradation Model, Energies, (2018), ISSN:1996-1073.

[44] Wahdame, B.; Candusso, D.; François, X.; Harel, F.; Péra, M.; Hissel, D.; Kauffmann, J.: Comparison between two PEM fuel cell durability tests performed at constant current and under solicitations linked to transport mission profile, International Journal of Hydrogen Energy 32: 4523-4536, (2007).

[45] Enz S.: Einfluss von hochdynamischen Betriebszuständen auf die Aktivkomponenten von Polymer-Elektrolyt-Membran-Brennstoffzellen. Dissertation Universität Ulm, 2015.

[46] Pei, P.; Chen, H.: Main factors affecting the lifetime of Proton Exchange Membrane fuel cells in vehicle applications: A review, Applied Energy, 125 (2014), 60-75.

[47] Storn, R.; Price, K.: Differential Evolution — a Simple and Efficient Heuristic for Global Optimization over Continuous Spaces, Journal of Global Optimization, 11 (1997), 341-359.

[48] Weicker, K.: Evolutionäre Algorithmen, Springer, ISBN: 978-3-658-09957-2, 2015.

[49] Rodriguez-Mier, P.: Website: https://pablormier.github.io, [Online] `https://pablormier.github.io/2017/09/05/a-tutorial-on-differential-evolution-with-python/`. Information accessed on 16.4.2021.

[50] Sorrentino, A.; Sundmacher, K.; Vidakovic-Koch, T.: Polymer Electrolyte Fuel Cell Degradation Mechanisms and Their Diagnosis by Frequency Response Analysis Methods: A Review, Energies, 13 (2020) p. 5825.